Master's Thesis

Highly reflective methyl acrylate/copolymer-TiO_2 hybrid one-dimensional photonic crystal sensor for colorimetric detection of solvents in adulterated gasoline

Minju Jeong

School of Energy and Chemical Engineering

(Energy Engineering)

Ulsan National Institute of Science and Technology

2023

Highly reflective methyl acrylate/copolymer-TiO_2 hybrid one-dimensional photonic crystal sensor for colorimetric detection of solvents in adulterated gasoline

Minju Jeong

School of Energy and Chemical Engineering

(Energy Engineering)

Ulsan National Institute of Science and Technology

Highly reflective methyl acrylate/copolymer-TiO_2 hybrid one-dimensional photonic crystal sensor for colorimetric detection of solvents in adulterated gasoline

A thesis/dissertation submitted to
Ulsan National Institute of Science and Technology
in partial fulfillment of the
requirements for the degree of
Master of Science

Minju Jeong

11.22.2022 of submission

Approved by

Advisor

Jongnam Park

Highly reflective methyl acrylate/copolymer-TiO_2 hybrid one-dimensional photonic crystal sensor for colorimetric detection of solvents in adulterated gasoline

Minju Jeong

This certifies that the thesis/dissertation of Jongnam Park is approved.

11.22.2022 of submission

Advisor: Jongnam Park

Chang Young Lee

Jong Mok Park

Abstract

Recently, the manufacture and distribution of adulterated gasoline mixed with pure commercial gasoline and adulterants has become a global problem. However, there is still a lack of a simple way to detect it immediately on-the-spot. In this study, we propose highly reflective one-dimensional photonic crystals (1D PC) as a simple, on-the-spot detection method for adulterated gasoline with the naked-eye. First, a photo cross-linked polymer–TiO_2 hybrid material (Ti70) with a high refractive index and P(MA-*co*-BPA) with a low refractive index were synthesized and analyzed. After that, they were used to fabricate a total of 11 layers of highly reflective Ti70/P(MA-*co*-BPA) 1D PC. The fabricated Ti70/P(MA-*co*-BPA) 1D PC exhibited purple in pristine and no color change was observed when immersed in pure commercial gasoline. On the other hand, when immersed in methanol, xylene, toluene, and benzene, the colors of Ti70/P(MA-*co*-BPA) 1D PCs changed rapidly to strong blue, blue, yellow-green, and orange, respectively. In addition, Ti70/P(MA-*co*-BPA) 1D PC showed color change within a short time (~10 s) even in binary or ternary solvent mixtures(gasoline-toluene, gasoline-methanol, gasoline-toluene-methanol). Moreover, the excellent reusability of Ti70/P(MA-*co*-BPA) 1D PC was verified through 10 repetitions of swelling-deswelling tests. Through these results, it was confirmed that the novel Ti70/P(MA-*co*-BPA) 1D PC can be successfully applied to the colorimetric on-the-spot detection of adulterated gasoline.

Blank page

Contents

Contents of scheme

Contents of Figure

Contents of Table

Nomenclatures

1D PC	one-dimensional photonic crystals
PCs	photonic crystals
HRIM	high refractive index material
LRIM	low refractive index material
PSB	photonic stop band
TiX	P(NIPAM-*co*-DA-*co*-BPA) and TiO_2 hybrid
NIPAM	N-isopropylacylamide
UV	ultraviolet
RT	room temperature
DH	dopamine hydrochloride
DA	dopamine acrylamide
BPAm	4-benzoylphenyl acrylate
P(NIPAM-*co*-DA-*co*-BPA)	poly(N-isopropylacrylamide-*co*-dopamine acylamide-*co*-4-benzoylphenyl acrylate)
P(MA-*co*-BPA)	poly(methyl acrylate-*co*-4-benzoylphenyl acrylate)
PDI	polydispersity index
DMSO	dimethyl sulfoxide
AIBN	azobisisobutyronitrile
PMMA	poly(methyl methacrylate)
std.	standard
***o*-xylene**	ortho-xylene
***m*-xylene**	metha-xylene
***p*-xylene**	para-xylene

GT mixture	gasoline and toluene mixture
GM mixture	gasoline and methanol mixture
GTM mixture	gasoline, toluene and methanol mixture

I. Introduction

1.1 Problems and status of adulterated gasoline use

The discovery and use of fossil fuels have revolutionized human civilization. However, oil prices are on the rise due to the depletion of reserves, competition for energy supremacy between countries, and war.[1, 2] Gasoline is one of the most widely used fossil fuels for transportation and power generation worldwide.[3, 4] Gasoline price increase can provide motivation for the manufacture and distribution of adulterated gasoline for illegal crimes. Adulterated gasoline can be made into pseudo-gasoline or adulterated gasoline by mixing pure commercial gasoline with waste organic solvents to avoid high oil prices, or by mixing inexpensive organic solvents, which are industrial solvents that are not subject to fuel tax.

As shown in **Figure 1**, the use of adulterated gasoline causes the internal combustion engine to malfunction or shorten its lifespan and increase the emission of harmful gases such as CO and NOx.[5, 6] It can also be used for economic crimes such as evading the national fuel tax and has a serious problem, so a thorough crackdown is necessary. Economic crimes using adulterated gasoline are crimes that profit from the mixing of high-tax pure commercial gasoline with low-tax adulterants. The damage caused by the distribution of adulterated gasoline was estimated at KRW 1.72.7 trillion in 2011 in Korea, over £500 million annually in the UK, and over 300 billion rupees per year in India.[7]

Commercial gasoline consists mainly of a mixture of aromatic and aliphatic hydrocarbons consisting of 4 to 12 carbons (C_4-C_{12}), and it has been known that adulterated gasoline is produced by adding inexpensive organic solvents such as methanol and toluene to pure commercial gasoline.[3, 7-10] Accurate analysis is possible if expensive analysis equipment such as gas chromatography (GC) is used to analyze the illegal composition of adulterated gasoline.[11] However, for effective detection on-the-spot, it is necessary to develop a detection technology that can easily and intuitively determine the authenticity.

Figure 1. Illustration explaining that the use of adulterated gasoline can cause environmental pollution, engine failure, and tax evasion.

1.2 Need for sensor development for detection of adulterated gasoline on-the-spot

Traditional high-precision methods such as GC, liquid chromatography (HPLC), spectroscopy and nuclear magnetic resonance (NMR) can be used to detect adulterated gasoline. However, these methods have the disadvantages of being time-consuming, expensive, and having to secure a place for storing huge instruments, so they cannot be used for the detection of adulterated gasoline on-the-spot.[9, 11-14]

As shown in **Table 1**, portable devices that can detect adulterated gasoline on-the-spot, such as near infrared light emitting diode based photometer, polydiacetylene based microfiber, organic fluorescent dyes, bimetallic nanoparticles, all organic one-dimensional photonic crystals (1D PC) sensor, have continued to be developed.[7, 15-20]

Although a variety of promising sensors for on-the-spot detection of adulterated gasoline have been reported so far, it is still necessary to develop sensors that are cheaper, simpler, smaller, more reliable, and capable of detecting various adulterants used on-the-spot.[11] 1D PC are one of the promising candidates that meet this condition.

Table 1. Comparison of portable devices for on-the-spot detection of adulterated gasoline.

Sensor type	Mechanisms	Features	Ref.
Near infrared light emitting diode based photometer	Detecting transmittance changes	Highly sensitive (> 3% adulterants) but only detectable when the concentration of one adulterant is higher than the other	6
Polydiacetylene based microfiber	Optical absorption changes	Sensing various volatile organic compounds (VOCs) in adulterated gasoline but poor color contrast (only blue and red)	7
Organic fluorescent dyes	Fluorescence color changes	Fast detection of adulterated gasoline but high cost due to the requiring additional instruments	16
Bimetallic nanoparticles	Optical absorption changes	Low detection limit (~1%) of adulterants in adulterated gasoline. Slow response rate (45-60 min) and poor visibility	17
All organic 1D PC sensor	Reflection color changes	Fast color changes (< 1 s) but poor reflectance (< 10%) for naked-eye detection	18-20
Polymer-TiO_2 hybrid 1D PC sensor	Reflection color changes	Colorimetric sensing of various VOCs with high reflectance (> 70%), fast color changes (< 5 s), and good reusability	This work

1.3 1D PC sensors for detection of adulterated gasoline

Photonic crystals (PCs) are nanostructures composed of two materials with different refractive indices and made periodically along one direction.[21-23] **Figure 2** shows a schematic diagram that can be structurally divided into PCs that can be seen in nature. As shown in **Figure 2a**, it can be seen that PCs have regular nanostructures like blue morpho butterfly wings, peacock feathers, chameleon skin, and mine stone.

PCs can be structurally divided into one-dimensional, two-dimensional, and three-dimensional structures (**Figure 2b**). Among them, 1D PC have the potential to be applied to various sensor fields because they are simpler, easier to fabricate, and more responsive to stimuli than others.[14]

1D PC are fabricated in periodic arrangements in the vertical direction of the surface using high refractive index material (HRIM) and low refractive index material (LRIM) with different refractive indices. Two materials (HRIM, LRIM) with different refractive indices allow or inhibit the propagation of incident light depending on the wavelength. Here, the range of forbidden wavelengths is called the photonic stop band (PSB). The PSB induces strong reflectance in wavelength regions defined as partial diffraction in 1D PC. Therefore, by periodically stacking colorless materials, a strong color (structural color) is obtained if the PSB is in the visible region of the spectrum, which can be seen with the naked-eye. The wavelength and reflectance of PSB peak of 1D PC can be predicted using Bragg's law (**Equation (1)**) and **Equation (2)**, respectively.[24]

$$\lambda_{max} = 2(n_l d_l + n_h d_h) \quad (1)$$

$$R = \left(\frac{1-Y}{1+Y}\right)^2 \times 100\%, \; Y = \left(\frac{n_h}{n_l}\right)^{N-1} \frac{{n_h}^2}{n_s} \quad (2)$$

n_h, n_l = refractive index of material ($n_h > n_l$)
n_s = refractive index of substrate
d_h, d_l = thickness of material
N = number of periodic

The wavelength of the 1D PC's first maximum reflection (λ_{max}) can be adjusted by varying the refractive index (n) and thickness (d) of HRIM and LRIM, respectively (**Equation (1)**). The reflectance (R), the intensity of the structural color at the first maximum reflection wavelength, is usefully adjusted by varying the refractive index difference ($\Delta n = n_h - n_l$), the number of periodic stacks (N) (**Equation (2)**).

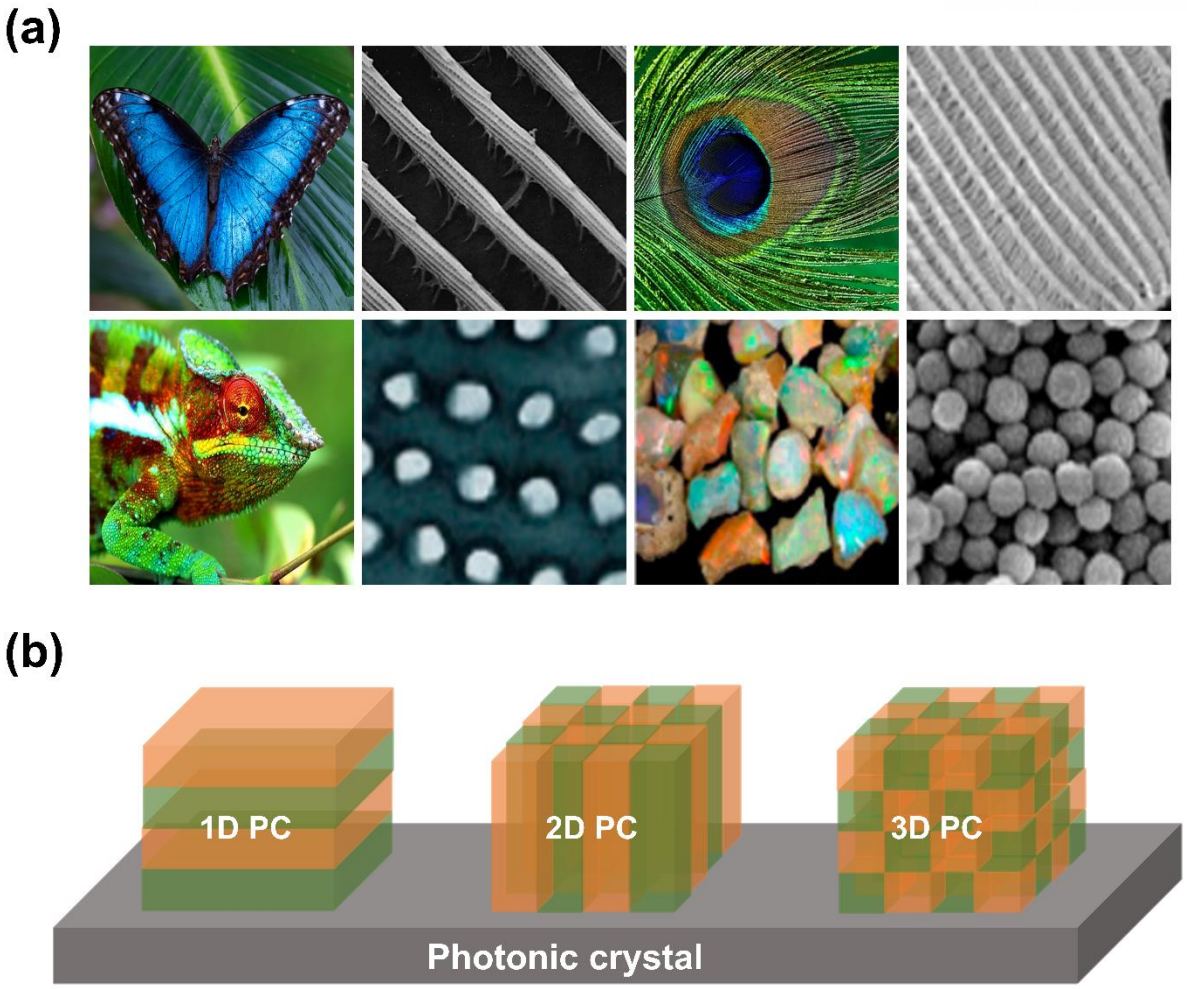

Figure 2. (a) Images and SEM images of blue morpho butterfly, peacock feathers, chameleon, mine stone with natural PCs,[25-30] (b) schematic diagrams of structural cycles in one-dimensional, two-dimensional and three-dimensional.

1.4 Development of novel polymer–TiO_2 hybrid material for highly reflective 1D PC sensor

The colorimetric 1D PC sensor has a structural color change when stimulation leads to a change in thickness. Using 1D PC, a cross-linked polymeric layer designed to exhibit swelling behavior by a specific analyte is applied. When the analyte penetrates into the cross-linked polymeric network, the thickness of the polymeric layer changes due to the swelling behavior, resulting in color change of the 1D PC sensor. Therefore, by using 1D PC sensor, a specific analyte can be colorimetrically detected with naked-eye.

Polymer-based 1D PCs have various functional groups, so it can control the responsiveness to external stimuli.[19, 20] However, since polymers have a relatively low refractive index, the 1D PC sensor composed only of polymers has the disadvantage of showing low reflectance due to Δn. 1D PC sensor with low reflectance is not easy to observe naked-eye, so 1D PC for use as a colorimetric sensor requires high reflectance. It can be used for 1D PCs composed of inorganic materials such as TiO_2 and SiO_2 for high reflectance.[31-33] Using inorganic materials, it is possible to efficiently fabricate 1D PCs with high reflectance in a small number of stacks due to a large Δn.[34]

A polymer-inorganic hybrid material that combines the strengths of polymer and inorganic material has optimal properties for use as HRIM. In the polymer-inorganic hybrid material, the inorganic component improves the refractive index and the polymer component forms a stable cross-linked network to improve the stability of 1D PC.[35] In addition, the compatibility with other materials can be improved by controlling the hydrophilicity/hydrophobicity of polymer-inorganic hybrid materials.[35, 36]

However, although these polymer-inorganic hybrid materials seem desirable for the development of 1D PC, it is not easy to fabricate uniform films due to poor compatibility between the polymeric-inorganic hybrid materials and other materials.[37] Therefore, research on the development of highly reflective 1D PCs with high durability and reliability using polymer-inorganic hybrid materials is still in the early stages.

1.5 Motivation

In this study, we attempted to develop a highly reflective 1D PC sensor that can detect colorimetrically with the naked-eye to distinguish between pure commercial gasoline and adulterated gasoline containing adulterants such as toluene and methanol.

First, we tried to develop a novel polymer-inorganic hybrid material with a high refractive index to obtain a large refractive index difference (Δn). The polymer-inorganic hybrid material was used as an HRIM and an acrylate-based LRIM was used to fabricate a 1D PC.

Since acrylate-based polymers exhibit swelling behavior by various organic solvents, the development of the highly reflective 1D PC sensor that changes color by various organic solvents is expected when this is applied to a 1D PC sensor.

In addition, the prepared HRIM and LRIM improved durability by including a photo-crosslinking system, and the 1D PC sensor was expected to indicate excellent reusability.[36]

To verify the performance in adulterated gasoline of the 1D PC sensor prepared to meet expectations, immersion in single solvents (pure commercial gasoline, methanol, xylene, toluene, benzene), binary mixtures (gasoline/methanol, gasoline/toluene), and ternary mixture (gasoline/toluene/methanol) explored changes in optical properties, response time, and reusability.

II. Experimental

2.1 General

Borax (sodium tetraborate decahydrate), sodium carbonate (Na_2CO_3), acryloyl chloride, methyl acrylate (MA), titanium(IV) propoxide were purchased from Sigma-Aldrich (USA). Dopamine hydrochloride, *N*-isopropylacrylamide (NIPAM) and azobisisobutyronitrile (AIBN) were purchased from Tokyo Chemical Industry (Japan). 4-benzoylphenyl acrylate (BPAm) was purchased from RND Korea Co. (Korea). Pure commercial gasoline was purchased from SK Energy Co. (Korea) and S-Oil Co. (Korea) and used as received. The compositions of commercial gasoline were measured by Agilent 7890 A Series gas chromatography (GC) equipped with flame ionization detector (FID). GC analysis was performed using an Agilent HP-5 capillary column (30 m × 0.32 mm) with a film thickness of 0.25 μm. The flow rate of FID was fixed at 16.83 mL/min for N_2 and H_2 35 mL/min and air 350 mL/min. During the GC analysis, the initial temperature of the oven was at 34 °C for 10 min, followed by a temperature program that ramped up at a rate of 5 °C/min to 230 °C for 5 min. All other chemicals were used without purification and were purchased from commercial suppliers. A transparent glass substrate was purchased from NTP Inc. (Korea). Monomer (DA) and copolymers (P(NIPAM-*co*-DA-*co*-BPA)), P(MA-*co*-BPA)) were synthesized following reported procedure.[38-40] The film samples were UV exposed using a Matsushita MS-3501MF belt conveyor UV curing system equipped with a high-pressure Hg lamp. The UV exposure was 1250 mJ/cm2 for each irradiation cycle. UV has a wavelength range of 280-400 nm (UV-B and UV-C) and peaks at 365 nm. ^{1}H nuclear magnetic resonance (NMR) were measured by Bruker Avance III 300 (300 MHz) spectrometer. The average molecular weight (M_w), polydispersity index (PDI), and number average molecular weight (M_n) were measured by gel permeation chromatography (GPC) using an Agilent Technologies 1260 Infinity series instrument equipped with two Agilent PLgel 5 μm MIXED-D × 7.5 mm columns and a refractive index detector. GPC was used with dimethylformamide eluent of 0.01M Lithium bromide in poly methyl methacrylate (PMMA) standard at 40℃ and flow rate of 1 mL/min. Thermogravimetric (TG) curves using a TA Instruments Q500 were measured in an O_2 atmosphere with a heating rate of 20 °C/min. Differential scanning calorimetry (DSC) using TA Instruments Q2000 was measured in N_2 atmosphere at a heating rate of 20 °C/min. Fourier transform infrared (FTIR) spectra using a Thermo Fisher Scientific Nicolet 6700 spectrometer were performed in attenuated total reflection mode. The thickness and refractive index of thin films using a Horiba UVISEL LT-FGMS spectroscopic phase modulation ellipsometer were measured at 75˚ of incidence angle. The 75˚ of incidence angle was adapted to maximize the sensitivity of the sample placed on the Si wafer near the Brewster angle. The reflectance, contour plot, and reproducibility tests of a 1D PC sensor using an Ocean Optics USB4000-UV-VIS-ES spectrometer were measured at 0˚ of incidence angle. The image of gel, color change of 1D PC sensor were obtained using Apple iPhone 12 Pro and Samsung Galaxy Z Flip 3. The cross-sectional scanning electron

microscopy (SEM) samples using the FEI Helios NanoLab 450 focused ion beam (FIB)/SEM dual beam instrument improved the conductivity of the samples prior to fabrication. During sample preparation, the samples were coated with Pt and vitreous C by sputtering to reduce potential damage to these samples due to the ion beam. The SEM instrument of the FEI Helios NanoLab 450 dual beam system measured cross-sectional SEM images of the samples.

2.2 Synthesis of materials

2.2.1 Dopamine acrylamide, DA

The whole process was done in the absence of UV light. DA was synthesized according to a previously reported procedure.[41] Borax (40.2 g, 105.40 mmol), sodium carbonate (16.8 g), deionized water (1500 mL) were added into a 3-neck round-bottom flask. This solution was degassed in a sonicator bath for 60 min under 100 mbar vacuum. Dopamine hydrochloride (10 g, 52.73 mmol) was added into the degassed solution under nitrogen atmosphere and the resulting solution was stirred for 2h at RT. The prepared solution was cool to 3 ℃, then, acyloyl chloride (12.9 mL, 158.20 mmol) was slowly added dropwise into the resulting solution. Thereafter, another sodium carbonate (16.8 g) was added into reaction solution to maintain the pH 9 and stirring for 16h at RT. The solution was acidified to pH 2 with 6N HCl solution and stirred for 60 min. The residue was dissolved in ethyl acetate and washed twice with 0.1N HCl solution and brine and drying with $MgSO_4$. The solvent was removed by a vacuum evaporator at 40 ℃ and purified by silica gel column chromatography with methanol : dichloromethane = 1 : 9 (*v/v*) mixture as an eluent. Finally, DA was obtained as a white powder (7.44 g, yield : 55%).

^{1}H NMR (300 MHz, DMSO, δ (ppm)) : 8.78 (s, O-*H*, 1H), 8.68 (s, O-*H*, 1H), 8.17-8.13 (t, *J* = 6Hz, C=O-N*H*, 1H), 6.65-6.62 (d, *J*=9Hz, aromatic, 1H), 6.59-6.58 (d, *J* = 3Hz, aromatic, 1H), 6.46-6.42 (dd, *J* = 9Hz, aromatic, 1H), 6.25-6.16 (dd, *J* = 18Hz, -C=C-*H*, 1H), 6.10-6.03 (dd, *J* = 18Hz, (trans)H_2-C=CH-C=O, 1H), 5.59-5.55 (dd, *J* = 10.5Hz, (cis)H_2-C=CH-C=O, 1H), 3.30-3.23 (t, *J* = 7.5Hz, NH-C-H_2, 2H), 2.58-2.55 (t, *J* = 7.5Hz, NH-CH_2-C-H_2, 2H).

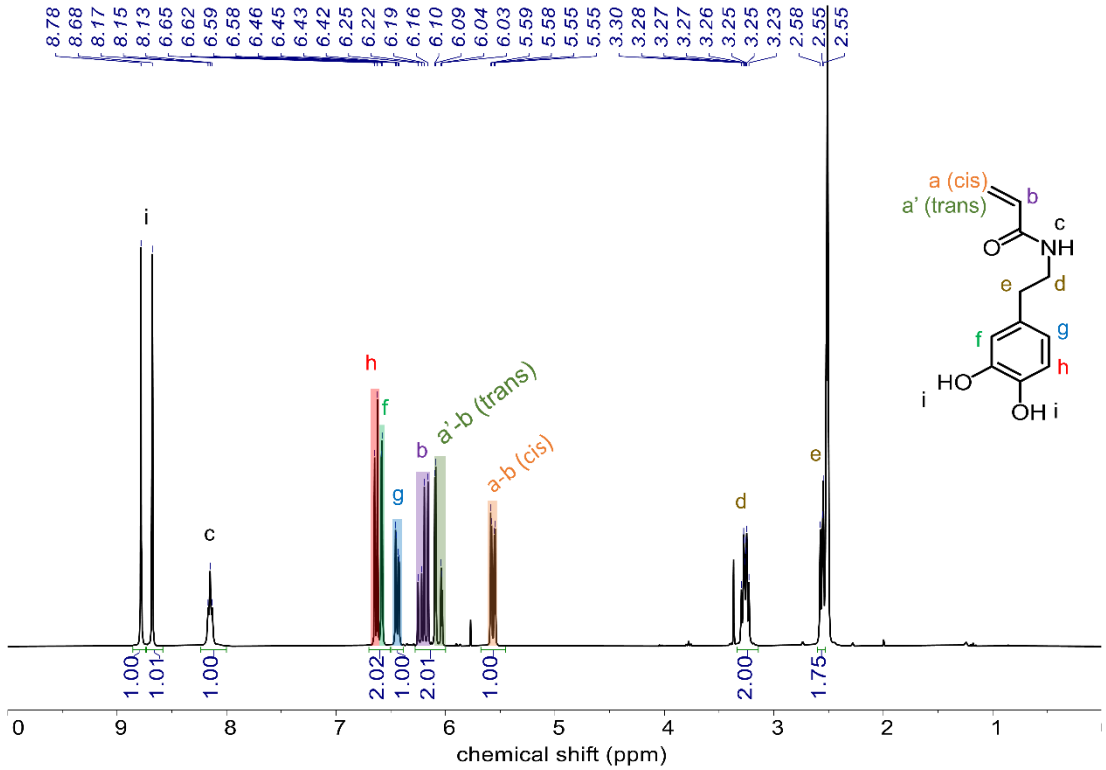

Figure 3. ^{1}H-NMR (300 MHz) spectrum of DA in DMSO.

2.2.2 Poly(N-isopropyl acrylamide-*co*-dopamine acrylamide-*co*-4-benzoylphenyl acrylate), P(NIPAM-*co*-DA-*co*-BPA)

The whole process was done in the absence of UV light. P(NIPAM-co-DA-co-BPA) was synthesized according to a previously reported procedure.[42] In the schlenk flask equipped with a magnetic bar, N-isopropyl acrylamide (NIPAM) (4.9145 g, 43.43 mmol), DA (1 g, 4.83 mmol), 4-benzoylphenyl acrylate (BPAm) (0.6087 g, 2.41 mmol), azobisisobutyronitrile (AIBN) (0.0832 g, 0.51 mmol) were dissolved in 66 mL of methanol. The flask was followed by nitrogen bubbling for 10 min. Then, the reaction solution was placed in an oil bath, and stirred under nitrogen atmosphere for 18h at 70 ℃. The reaction was quenched by removing the flask from the oil bath and exposing it to air. The solution poured into ethyl ether to precipitate the reaction solution, and the precipitated copolymers were collected by filtration under reduced pressure. The obtained copolymers were dried in a vacuum oven for 24 h at RT. Finally, P(NIPAM-*co*-DA-*co*-BPA) was obtained as a white solid (5.3 g, yield : 81%).

^{1}H NMR (300 MHz, DMSO, δ (ppm)) : 8.81-8.66 (m, O-*H*, 2H), 7.69-7.21 (m, -N-*H*-CH(CH_3)(CH_3), -N-*H*-CH_2-CH_2-$C_6H_3(OH)_2$, -C_6-*H*$_4$-C(=O)-C_6-*H*$_5$, 11H), 6.61-6.40 (m, -C_6-*H*$_3$($OH)_2$, 3H), 3.84 (s, -NH-C-*H*(CH_3)(CH_3), 1H). The ratio of P(NIPAM-*co*-DA-*co*-BPA) was estimated as 84.2 : 11.5 : 4.3 by ^{1}H NMR. M_n = 66,100 g/mol, PDI (polydispersity) : 2.1 was given by GPC (PMMA std.).

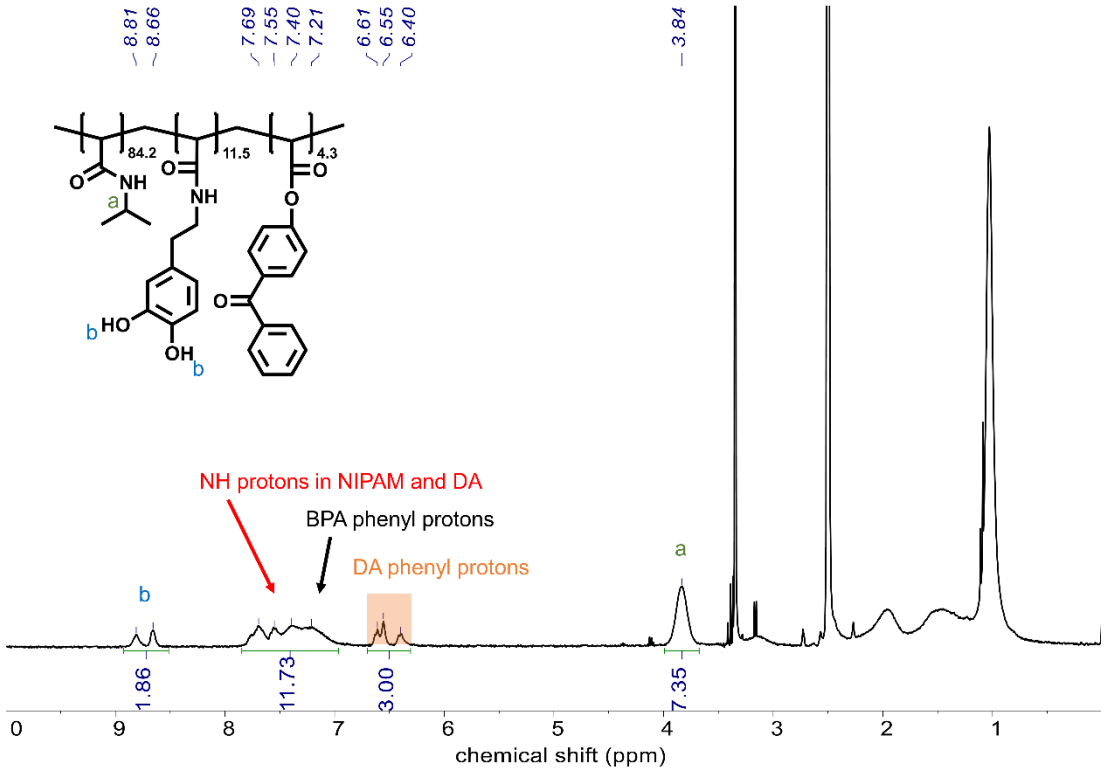

Figure 4. [1]H-NMR (300 MHz) spectrum of P(NIPAM-*co*-DA-*co*-BPA) in DMSO.

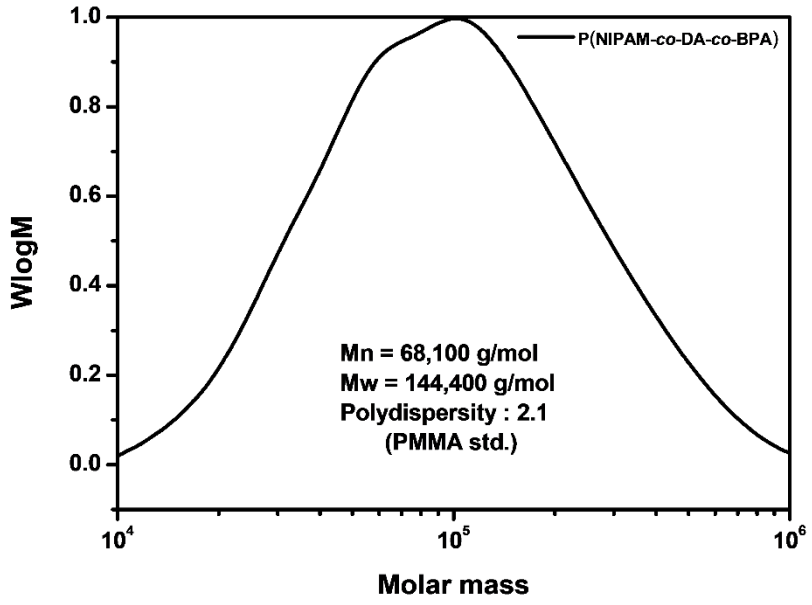

Figure 5. GPC traces of P(NIPAM-*co*-DA-*co*-BPA) in PMMA standard.

2.2.3 Poly(Methyl acrylate-*co*-4-benzoylphenyl acrylate), P(MA-*co*-BPA)

The whole process was done in the absence of UV light. In the schlenk flask equipped with a magnetic bar, methyl acrylate (MA) (10 g, 116.16 mmol), 4-benzoylphenyl acrylate (BPAm) (0.2930 g, 1.17 mmol), azobisisobutyronitrile (AIBN) (0.01926 g, 0.12 mmol) were dissolved in 41 mL of dimethylformamide. The flask was followed by nitrogen bubbling for 10 min. Then, the reaction solution was placed in an oil bath, and stirred under nitrogen atmosphere for 18h at 70 ℃. The reaction was quenched by removing the flask from the oil bath and exposing it to air. The solution poured into ethanol to precipitate the reaction solution and dried. Then, secondary precipitation was performed in hexane, and the precipitated copolymers were collected by filtration under reduced pressure. The obtained copolymers were dried in a vacuum oven for 24h at RT. Finally, P(MA-*co*-BPA) was obtained as a white solid (7.4 g, yield : 72%).

^{1}H NMR spectrum (300 MHz, $CDCl_3$, δ (ppm)) : 7.87-7.47 (m, 9H, O-C_6H_4-(C=O)-C_6H_5), 3.66 (s, br, 25H, (C=O)-O-CH_3). The ratio of P(MA-*co*-BPA) was estimated as 99 : 1 by ^{1}H NMR. M_n = 66,100 g/mol, PDI : 2.1 was given by GPC (PMMA std.).

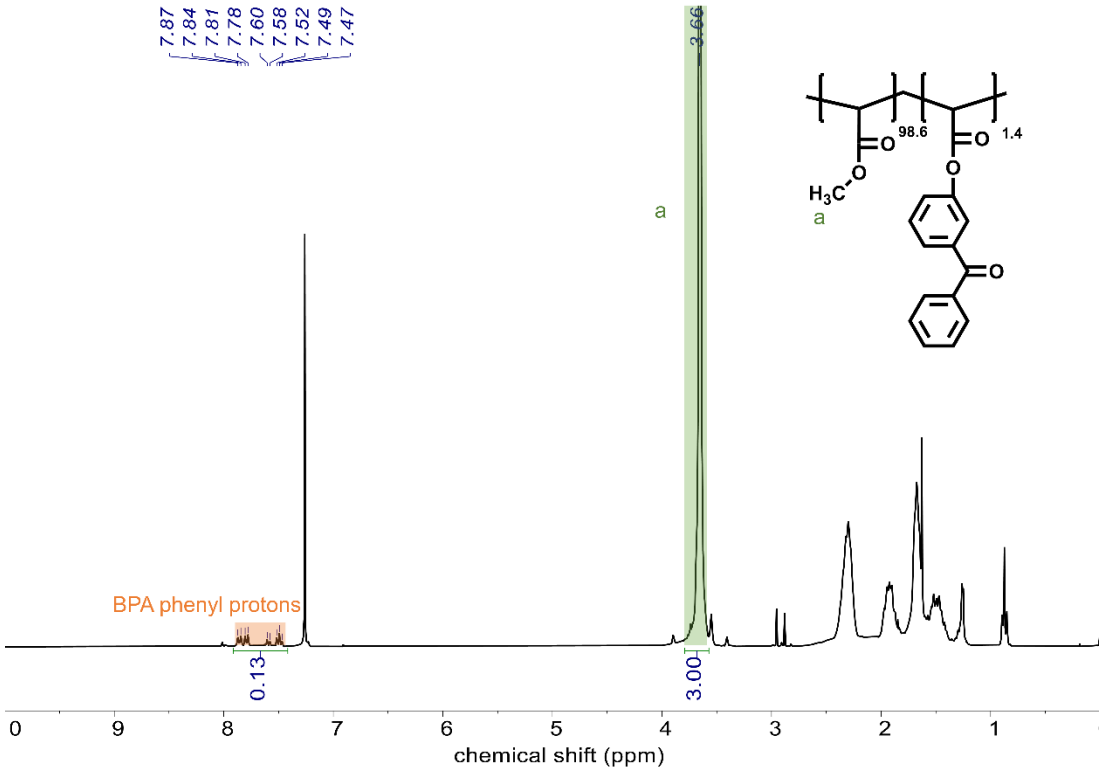

Figure 6. ^{1}H-NMR (300 MHz) spectrum of P(MA-*co*-BPA) in $CDCl_3$.

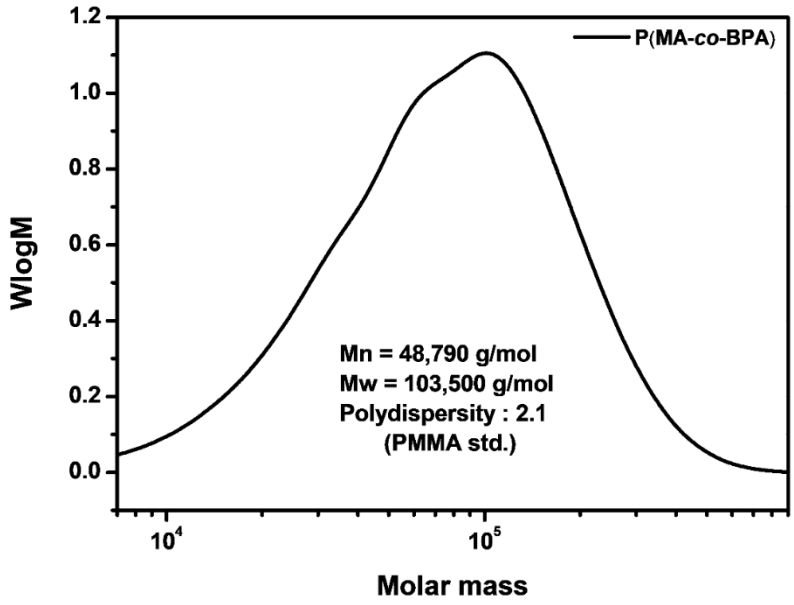

Figure 7. GPC traces of P(MA-*co*-BPA) in PMMA standard.

2.3 Preparation of P(NIPAM-*co*-DA-*co*-BPA) and TiO_2 hybrid (TiX) solutions

The whole process was done in the absence of UV light. The TiX solution was synthesized according to a previously reported procedure.[43-46] To illustrate the general synthesis process, the synthesis of copolymer-TiO_2 hybridized Ti70 (70; TiO_2 weight content relative to copolymer) was used as an example. The TiO_2 solution and the copolymer solution should be prepared separately for hybridization. The TiO_2 solution was stirred in 6 mL of propanol with 1.661 g of titanium(IV) propoxide in a vial with a magnetic bar at RT. The copolymer solution was stirred with 2 g of P(NIPAM-*co*-DA-*co*-BPA) in 10 mL of propanol at RT. The copolymer solution was slowly added dropwise to the TiO_2 solution. Then, 20 μL of 1 M HCl solution was added to 2 mL of propanol to dilute, put into a vial containing TiO_2 and a copolymer, and stirred at RT for 30 minutes. Finally, a red transparent liquid, copolymer- TiO_2 hybrid Ti70 was obtained.

2.4 Synthesis of Ti70 and P(MA-*co*-BPA) dry gels

The whole process was done in the absence of UV light. For Ti70 gel, 3.3 wt% of Ti70 solution was poured into a PTFE dish and the dish was exposed to UV irradiation for 30 min. Then, the Ti70 gel obtained from the PTFE dish was dried in an oven at 80 °C for 24 h. For P(MA-*co*-BPA) gel, 10 wt% of P(MA-*co*-BPA) was dissolved in toluene solution, placed in a transparent vial, sealed, and UV-irradiated for 1 h. After that, the vial was removed to obtain a P(MA-*co*-BPA) gel. Before use for swelling behavior analysis, the prepared dry gels were immersed in tetrahydrofuran or toluene several times to remove unreacted starting materials.

2.5 Swelling behavior analysis

Ti70 and P(MA-*co*-BPA) dry gels were separately immersed in pure commercial gasoline, methanol, xylene, toluene and benzene at RT. Remove the swollen gel from the solvent, remove the solvent on the surface, and weigh it. The swelling rate was calculated by the **Equation (3)**.[47]

$$\text{Swelling ratio } (\%) = \frac{W_{swollen} - W_{dry}}{W_{dry}} \times 100 \qquad (3)$$

$W_{swollen}$ = weight of the swollen gel.

W_{dry} = weight of the dry gel.

2.6 Thin film fabrication

Si wafers were cleaned using standard Radio Corporation of America cleaning methods.[48] The Ti70 thin film was prepared by spin-coating 50 μL of a Ti70 solution on a Si wafer at 6000 rpm for 30 s. The P(MA-*co*-BPA) thin film was prepared by spin-coating a solution of 3.0 wt% of P(MA-*co*-BPA) in toluene with 50ul on a Si wafer at 4000 rpm for 30 s. The P(MA-*co*-BPA) thin film with a thickness of 80-84 nm was obtained.

2.7 Assembly of the 1D PC sensor

A transparent polyethylene terephthalate (PET) film with a thickness of 80 μm was attached on glass with a thickness of 1.1 mm. After that, a dark polyvinyl chloride (PVC) film (transmission in the visible wavelength range: 5%) with a thickness of 35 μm was attached on top to make a basic film used for the sensor. On the base film, 100 μL of Ti70 solution was spin-coated at 6000 rpm for 30 s. After exposing the film to UV irradiation (1250 mJ/cm^2) at a rate of 2.0 M/min, dried it in an oven at 50 °C for 10 min. After that, cooled at room temperature for 10 min and spin-coated 100 μL of a solution of 3 wt% P(MA-*co*-BPA) in toluene as the next layer at 4000 rpm for 30 seconds. Repeated this process to fabricate 11 layers Ti70/P(MA-*co*-BPA) 1D PC. The glass with a thickness of 1.1 mm was used to protect the 1D PC sensor during spin-coating and was removed after all processes were completed.

III. Result and discussion

3.1 Design concept of synthesized materials

A high refractive index polymer and a low refractive index polymer were synthesized for use in the fabrication of 1D PC sensors. **Scheme 1** represents the synthesis process of prepared materials. P(NIPAM-*co*-DA-*co*-BPA) and P(MA-*co*-BPA) were synthesized using free radical polymerization.

Scheme 1a shows a synthesis process TiX (X=0, 10, 30, 50, 70, 100; weight content of TiO_2 compared to copolymer), HRIM prepared by hybridization of TiO_2 and P(NIPAM-*co*-DA-*co*-BPA). TiX were obtained by hybridizing the catechol group of DA contained in the P(NIPAM-*co*-DA-*co*-BPA) structure with TiO_2. Also, in the hydrophilic environment due to the presence of NIPAM, P(NIPAM-*co*-DA-*co*-BPA) could exhibit excellent stability and hydrophilicity during hybridization with TiO_2.[49, 50] The neat P(NIPAM-*co*-DA-*co*-BPA) that did not contain TiO_2 was indicated as Ti0.

Scheme 1b is the synthesis of P(MA-*co*-BPA) based on methyl acrylate used as LRIM. Acrylate polymers exhibit high swelling property in various organic solvents except hydrocarbon, which are the main component of gasoline, so they are expected to be able to detect adulterants contained in adulterated gasoline by applying them to 1D PC.[51, 52] BPA, commonly contained in P(NIPAM-*co*-DA-*co*-BPA) and P(MA-*co*-BPA), were used in 1D PC fabrication as photo cross-linking unit to form cross-linked networks of film.

1D PCs with BPA prevented decomposition or dissolution upon repeated exposure to solvents.[36]

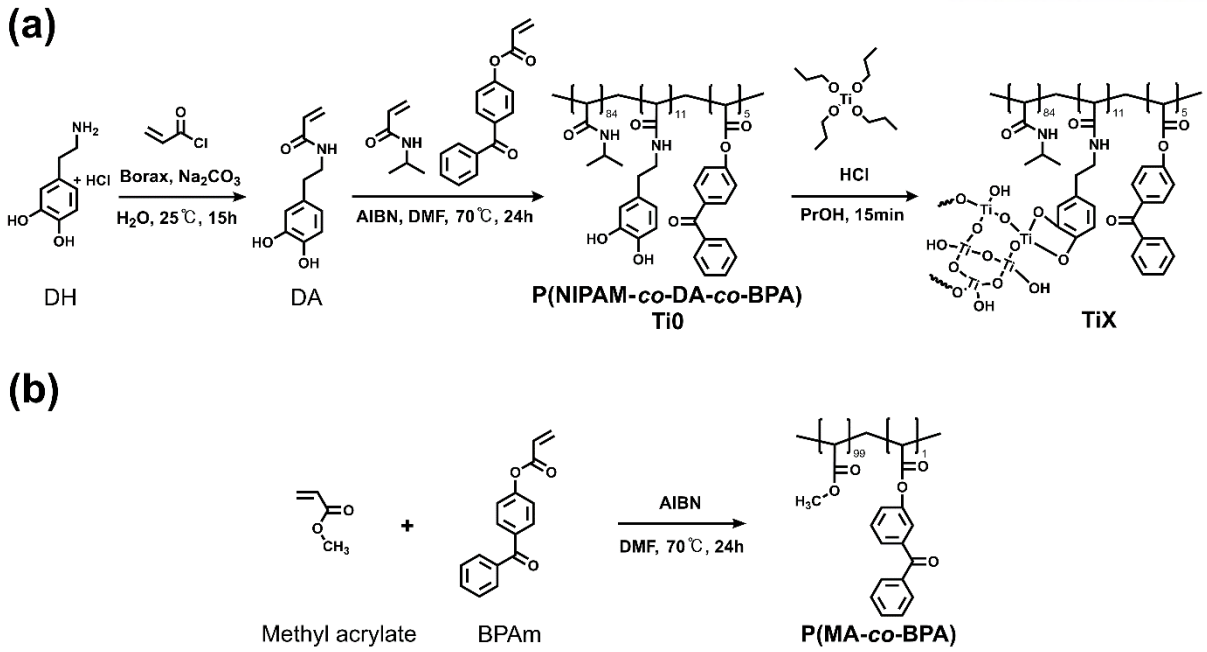

Scheme 1. (a) Synthesis of TiX as high refractive index material and (b) P(MA-*co*-BPA) as low refractive index material.

3.2 Characterization of refractive index controllable TiX

The synthesis of TiX was confirmed by thermogravimetric analysis (TGA), Fourier-transform infrared spectra (FT-IR), and spectroscopic ellipsometry. **Figure 8** shows the results of thermogravimetric curves and Fourier-transform infraded spectra of TiX. TGA was performed at a heating rate of 20 °C/min up to 800 °C in oxygen atmosphere. As shown in **Figure 8a**, Ti0 was completely decomposed by heat around 650 °C, indicating that the remaining weight percent was 0. On the other hand, the remaining weight percent of Ti100 was observed even after 650 °C. These results indicated that TiO_2 remained intact even after 650 °C. Therefore, it was confirmed from the TGA result that the remaining weight observed after 650 °C was the weight content ratio of TiO_2 contained in TiX.[46] **Table 2** summarized the theoretical values and TGA results of the weight content ratio of TiO_2 in TiX formed compared to the injected copolymer and $Ti(OPr)_4$. After 650 °C, the residual weights of Ti0, Ti10, Ti30, Ti50, Ti70 and Ti100 were 0%, 10.4%, 31.2%, 46.6%, 66.7% and 100%, respectively. These results were confirmed that the remaining weight of TiO_2 included in TiX almost identical to the theoretically calculated result (**Table 2**). **Figure 8b** shows the FT-IR spectra of TiX. Ti0 exhibited O–H stretching and N–H stretching of DA at 3000-3500 cm^{-1}, C=O stretching and N–H bending at 1650-1530 cm^{-1}. In addition, strong signals of Ti–O–Ti, Ti–O–C bonding peaks exhibited broad in the range of 500-800 cm^{-1}, and their signal strength increased with increasing content of TiO_2.[46, 53] The refractive indices of a TiX thin film on a silicon wafer were investigated using a spectroscopic ellipsometer in the range of 300-800 nm (**Figure 9**). As shown in **Figure 9a**, it was observed that the refractive indices of TiX increased with increasing TiO_2 contents. In particular, the refractive indices of TiX at 633 nm wavelength were analyzed as 1.49 (Ti0), 1.56 (Ti10), 1.62 (Ti30), 1.66 (Ti50), 1.71 (Ti70) and 1.78 (Ti100), respectively (**Figure 9b**).

As a result, it was confirmed that TiX was successfully synthesized as expected through the above analysis results. In addition, the refractive index of the TiX thin film can be easily controlled by adjusting the TiO_2 content in TiX.[46]

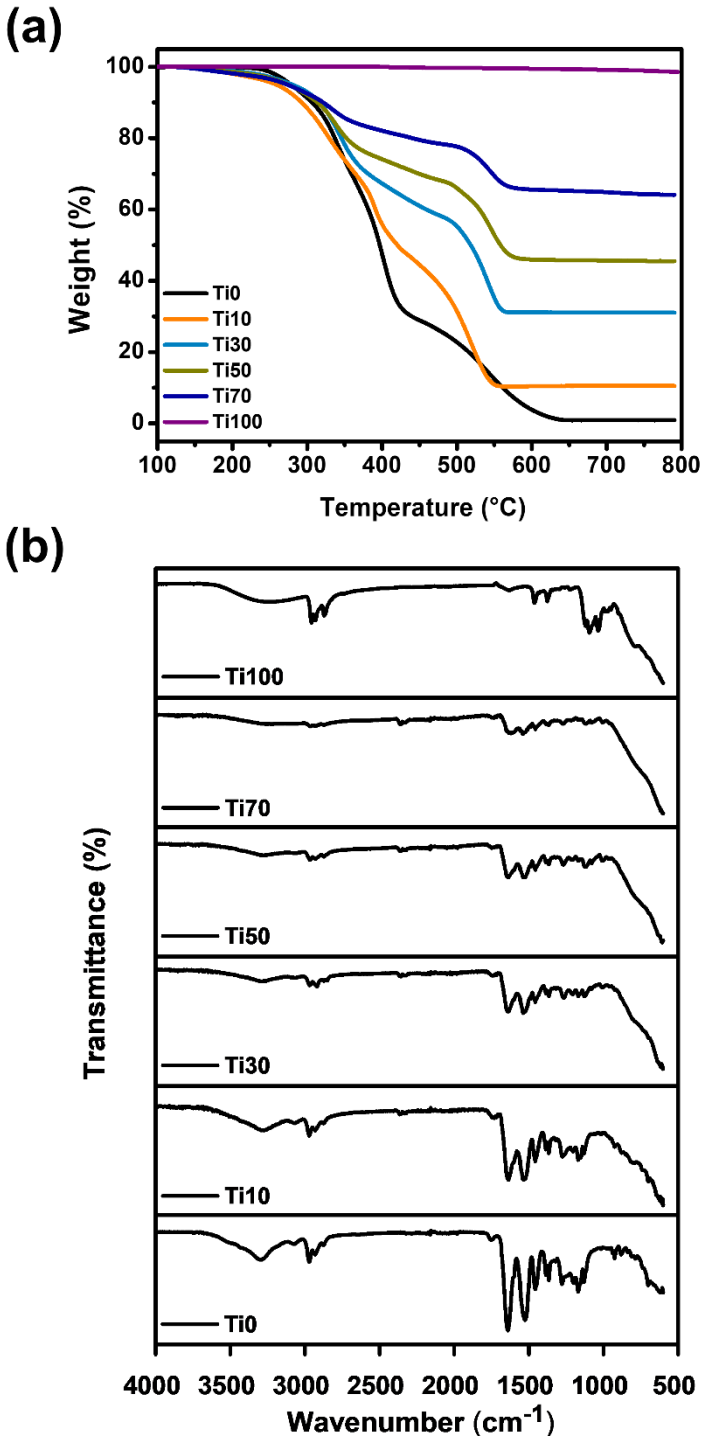

Figure 8. (a) Thermogravimetric curves of TiX under O_2 atmosphere and (b) FT-IR of TiX in the 4000-500 cm^{-1} range.

Table 2. Reactant composition of TiX, theoretical amount of hybrid material TiO_2 composition, and experimental amount measured by TGA.

TiX[a]	Reactant composition/wt%		Hybrid material TiO_2 composition/wt%	
	Copolymer[b]	$Ti(OPr)_4$	Theoretical	Experimental[c]
Ti0	100.0	0.0	0.0	0.0
Ti10	71.7	28.3	10.0	10.4
Ti30	39.6	60.4	30.0	31.2
Ti50	21.9	78.1	50.0	46.6
Ti70	10.7	89.3	70.0	66.7
Ti100	0.0	100.0	100.0	100.0

[a] In TiX, X is the weight content of TiO_2 compared to copolymer.
[b] P(NIPAM-*co*-DA-*co*-BPA) with a molar ratio of 9:1:0.02.
[c] Experimental TiO_2 composition was analyzed from the thermogravimetric analysis.

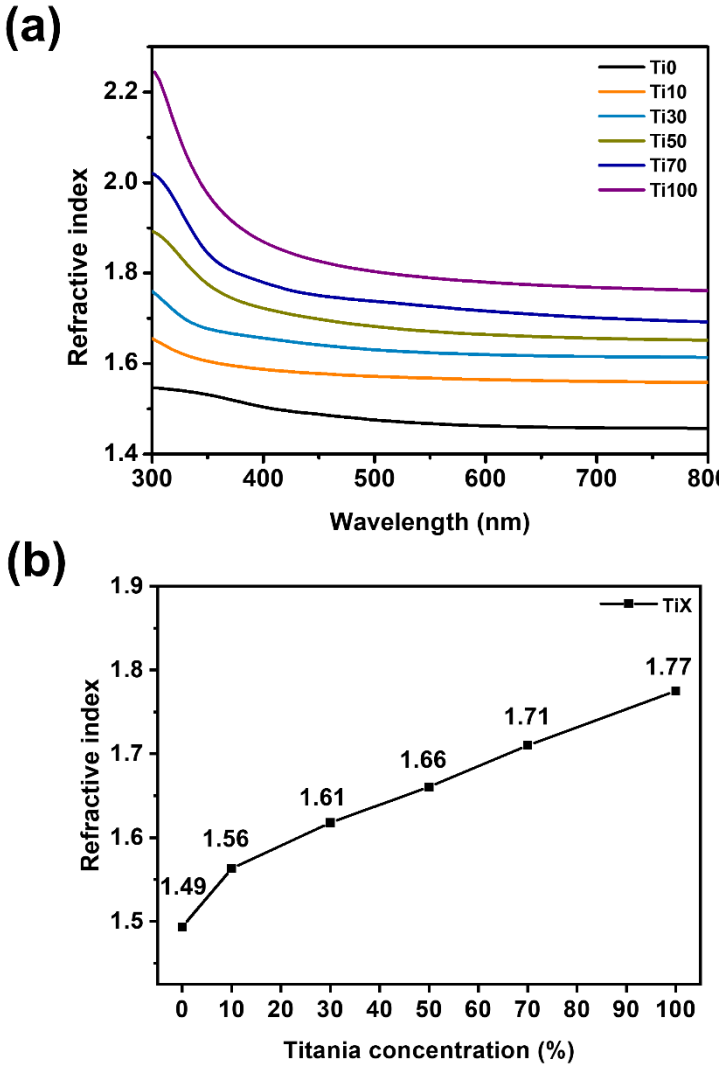

Figure 9. According to TiX contents (a) refractive index from 300 nm to 800 nm wavelengths and (b) refractive indices at 633 nm.

3.3. Fabrication of the 1D PC films

Before fabricating the 1D PC, the refractive indices of the synthesized materials were measured using a spectroscopic ellipsometer. The refractive indices of Ti0, Ti50, Ti70, and P(MA-*co*-BPA) from 300 nm to 800 nm wavelengths are shown in **Figure 10**. At the wavelength of 633 nm, the refractive indices of Ti0, Ti50, Ti70, and P(MA-*co*-BPA) were analyzed to be 1.48, 1.66, 1.71 and 1.51, respectively. Three types of 1D PCs (Ti0/P(MA-*co*-BPA), Ti50/P(MA-*co*-BPA) and Ti70/P(MA-*co*-BPA)) with different Δn were fabricated by alternately stacking LRIM and HRIM in one direction through spin-coating (**Figure 11a**). As shown in **Figure 11b**, when three types of 1D PCs were fabricated, HRIM was coated on the substrate first, and LRIM and HRIM were stacked on a total of 11 layers. The three types of 1D PCs adjusted the thickness of HRIM and LRIM as shown in **Table 3** based on Bragg's Law (**Equation (1)**), and the three types of 1D PCs produced the same reflection color in the pristine. The PSB peaks were made similar by setting the thickness of P(MA-*co*-BPA) commonly used in 1D PC to be the same and adjusting the thickness of Ti0, Ti50, and Ti70. The wavelengths of the three 1D PC PSB peaks fabricated require a minimum of 11 layers of stacking to produce reliable high reflectance visible to the naked-eye. However, the total number of stacks larger than 11 layers was not considered as it can increase the reflectance of 1D PCs but lower reproducibility.

In addition, when TiX with a high TiO_2 content was applied as HRIM, the difference in refractive index with LRIM increased, so that the reflectance of 1D PC can be increased. However, if the TiO_2 contents of TiX exceeded 70 wt%, it was precipitated during the fabricating of 1D PC and cannot be used. Ti0/P(MA-*co*-BPA) 1D PC had 8% reflectance at 402 nm, Ti50/P(MA-*co*-BPA) 1D PC had 40% reflectance at 394 nm, Ti70/P(MA-*co*-BPA) 1D PC had 74% reflectance at 393 nm (**Figure 12a**). The refractive index difference (Δn) of the HRIM and LRIM used in 1D PC increased from 0.03 to 0.2, increasing the reflectance from 8% to 74% at the PSB peak wavelength. The result can be explained by the increase in reflectance as Δn increases, as shown in **Equation (2)**.

Among the fabricated 1D PCs, Ti70/P(MA-*co*-BPA) 1D PC had the highest reflectance, making it suitable for use as an optical sensor for naked-eye detection. Therefore, additional detailed optical analysis was performed using a Ti70/P(MA-*co*-BPA) 1D PC. In addition, as a result of analyzing the cross-section of Ti70/P(MA-*co*-BPA) 1D PC through cross-sectional SEM image, it was confirmed that the Ti70 layer and the P(MA-co-BPA) layer were stacked evenly and periodically (**Figure 12b**). The thicknesses of Ti70 and P(MA-*co*-BPA) layers were analyzed to be 37.5±0.7 nm and 80.5±5.7 nm, respectively.

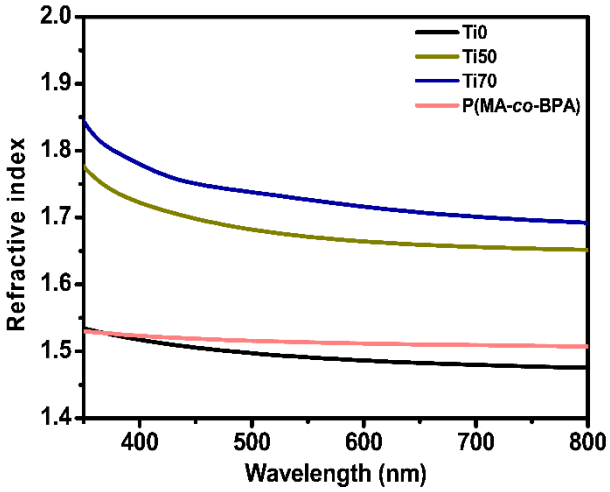

Figure 10. Refractive indices according to wavelengths from 300 nm to 800 nm of Ti0, Ti50, Ti70, P(MA-*co*-BPA).

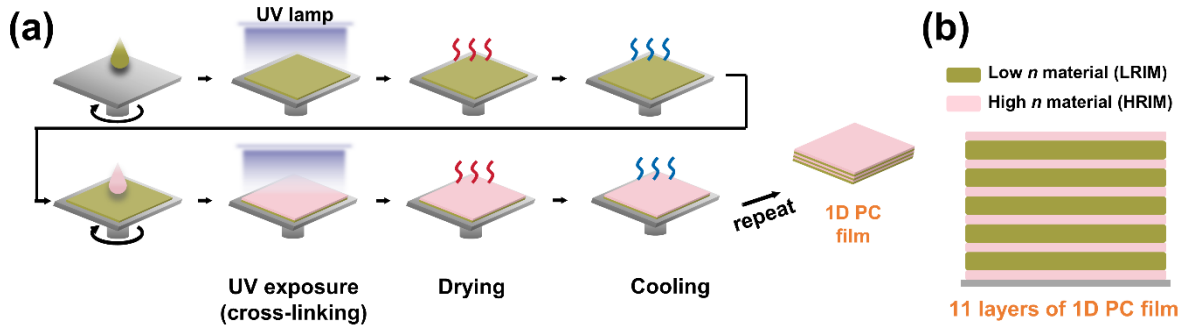

Figure 11. (a) 1D PC film fabrication by spin coating, (b) HRIM and LRIM were periodically cross-laminated for a total of 11 layers 1D PC film.

Table 3. Refractive indices and thicknesses of HRIM and LRIM, the difference in refractive index between HRIM and LRIM, reflectance in PSB of Ti0/P(MA-*co*-BPA), Ti50/P(MA-*co*-BPA), and Ti70/P(MA-*co*-BPA) 1D PC.

	HRIM (n^a, d^b)	LRIM (n^a, d^b)	Δn	Reflectance at PSB peak
Ti0/P(MA-*co*-BPA) 1D PC	P(MA-*co*-BPA) (1.51, 80.7±1.4 nm)	Ti0(1.49, 42.3±0.4 nm)	0.02	8% at 402 nm
Ti50/P(MA-*co*-BPA) 1D PC	Ti50(1.66, 40.2±1.3 nm)	P(MA-*co*-BPA) (1.51, 79.2±7.3 nm)	0.15	40% at 394 nm
Ti70/P(MA-*co*-BPA) 1D PC	Ti70(1.71, 37.5±0.7 nm)	P(MA-*co*-BPA) (1.51, 80.5±5.7 nm)	0.20	74% at 393 nm

[a] Refractive indices of layers analyzed using spectroscopic ellipsometer.
[b] Thickness of each layer in Ti0/P(MA-*co*-BPA) and Ti50/P(MA-*co*-BPA) 1D PCs investigated using spectroscopic ellipsometer, and thickness of each layer in Ti70/P(MA-*co*-BPA) 1D PC analyzed using cross-sectional scanning electron microscopy images.

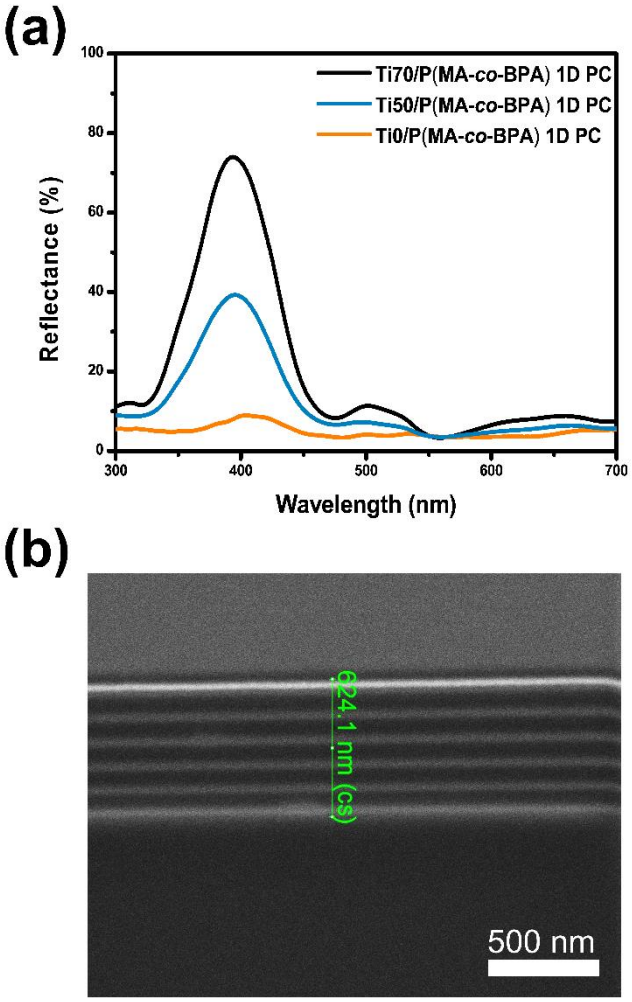

Figure 12. (a) Reflectance of Ti0/P(MA-*co*-BPA), Ti50/P(MA-*co*-BPA) and Ti70/P(MA-*co*-BPA) 1D PC, (b) SEM image of Ti70/P(MA-*co*-BPA) 1D PC.

3.4. Exploring the color change and swelling behavior of Ti70/P(MA-*co*-BPA) 1D PC

To analyze changes in optical properties, Ti70/P(MA-*co*-BPA) 1D PC was immersed in pure commercial gasoline, methanol, xylene, toluene, and benzene, respectively. Methanol, xylene, toluene, and benzene were selected as model adulterants that are widely used in the production of adulterated gasoline.[7]

GC results for pure commercial gasoline, hydrocarbon (n-hexane, n-heptane, n-octane, n-nonane, n-decane), methanol, benzene, toluene, and xylenes (*o*-xylene. *m*-xylene, *p*-xylene) standards are shown in **Figure 13**. As shown in **Figure 13**, it was confirmed that pure commercial gasoline to be used contains almost no adulterants such as methanol, benzene, toluene and xylenes. Acrylate polymers are known to exhibit swelling behavior by various organic solvents except for aliphatic hydrocarbons.[51] On the other hand, pure commercial gasoline is usually known to consist of aliphatic hydrocarbons.

Therefore, as depicted in **Figure 14**, we expected that Ti70/P(MA-*co*-BPA) 1D PC fabricated would exhibit color change differences between pure commercial gasoline and adulterated gasoline. Based on **Equation (2)**, Ti70/P(MA-*co*-BPA) 1D PC containing a P(MA-*co*-BPA) layers have no significant color changes when immersed in pure commercial gasoline (**Figure 14a**), but in adulterated gasoline containing adulterants such as methanol, xylene, toluene and benzene, it was expected that the color change would be large because the P(MA-*co*-BPA) layer thickness increases due to swelling (**Figure 14b**). Therefore, it was expected that adulterated gasoline can be detected with the naked-eye using the fabricated Ti70/P(MA-*co*-BPA) 1D PC.

Figure 15 exhibits the color change of Ti70/P(MA-*co*-BPA) 1D PC when immersed in pure commercial gasoline, methanol, xylene, toluene and benzene for 2 min. As shown in **Figure 15**, Ti70/P(MA-*co*-BPA) 1D PC presents little change in reflection color when immersed in pure commercial gasoline, but strong blue reflection color when immersed in methanol. And when Ti70/P(MA-*co*-BPA) 1D PC was immersed in xylene, toluene and benzene, it changed to blue, yellow-green, and orange within 0.5 s, respectively. The reflectance change of Ti70/P(MA-*co*-BPA) 1D PC immersed in pure commercial gasoline, methanol, xylene, toluene and benzene is shown in **Figure 16**. The reflectance spectra of Ti70/P(MA-*co*-BPA) 1D PC presented no significant change when immersed in pure commercial gasoline (**Figure 16a**). On the other hand, when Ti70/P(MA-*co*-BPA) 1D PC was immersed in methanol, its PSB peak wavelength shifted from 392 nm to 447 nm, and its reflectance slightly rose from the initial value (**Figure 16b**), and when immersed in xylene (**Figure 16c**), toluene (**Figure 16g**) and benzene (**Figure 16h**), its PSB peak wavelength shifted from 392 nm to 485 nm, 571 nm, and 660 nm, respectively, and the reflectance changed from the initial value of 74% to 56% (xylene), 49% (toluene), and 41% (benzene). The reflectance of Ti70/P(MA-*co*-BPA) 1D PC tends to decrease as the PSB shift due to swelling increases. The trends are presumably because the swelling breaks the

structural periodicity of Ti70/P(MA-*co*-BPA) 1D PC or causes defects. Therefore, the reflectance of Ti70/P(MA-*co*-BPA) 1D PC decreased significantly with increasing expansion of each layer. Also, when immersed in gasoline (**Figure 16d**), methanol (**Figure 16e**), xylene (**Figure 16f**), toluene (**Figure 16i**), and benzene (**Figure 16j**) of Ti70/P(MA-*co*-BPA) 1D PC, it can be observed through the contour plot that the reaction time all reach the saturated swelling wavelength within 10 s. The reflectance and wavelength of Ti70/P(MA-*co*-BPA) 1D PC were almost the same as the initial values even after repeated swelling 10 times, confirming excellent reusability (**Figure 16k**). When Ti70/P(MA-*co*-BPA) 1D PC swelled in benzene, the wavelength shifted a lot and the color change was clear and quick to respond, so it was selected for the reusability test. However, Ti70/P(MA-*co*-BPA) 1D PC demonstrated the same good reusability in gasoline, methanol, xylene and toluene.

$$\delta_t = \left(\frac{\Delta H_v - RT}{V_m}\right)^{1/2} \quad (4)$$

ΔH_v = heat of vaporization

R = ideal gas constant

T = temperature (K)

V_m = molar volume

The color change of Ti70/P(MA-*co*-BPA) 1D PC can be interpreted using **Equation (4)**.[54] The total solubility parameter (Hildebrand solubility parameter; δ_t) shown in **Equation (4)** is defined as the square root of the binding energy density, which is equal to the heat of vaporization of the compound divided by its molar volume (V_m). The heat of vaporization is proportional because of intermolecular interactions such as van der Waals forces. The solubility of a polymer depends on the difference between the δ value of the polymer and the δ value of the solvent. The smaller the difference, the more soluble the polymer is in the solvent, and the larger the difference, the less soluble the polymer is in the solvent. Although P(MA-*co*-BPA) used in this study contained a small amount of BPA (1.3 mol%), it was assumed that the δ value of P(MA-*co*-BPA) was the same as the methyl acrylate polymer, ignoring the influence of BPA.[52] As shown in **Table 4**, the δ differences ($\Delta\delta_{p\text{-}s}$) between P(MA-*co*-BPA) and pure commercial gasoline, methanol, xylene, toluene, and benzene were 3.1, 10.5, 1.1, 0.9, and 0.7, respectively. In addition, the molar volumes (V_m) of methanol, xylene, toluene and benzene were 40.5, 122.9, 106.9, and 89.4 cm3/mol, respectively.[55, 56] In **Figure 17**, P(MA-*co*-BPA) and Ti70 were made into gels and immersed in pure commercial gasoline, methanol, xylene, toluene, and benzene, respectively, to obtain a swelling ratio (**Equation (3)**) through weights when sufficiently swollen and dried. In the order of xylene, toluene and benzene, the swelling ratios of P(MA-*co*-BPA) gel were

1377%, 1881% and 2492%, respectively, with a tendency according to $\Delta\delta_{p\text{-}s}$, and in pure commercial gasoline, the swelling ratio of P(MA-*co*-BPA) gel was 22% (**Figure 17a**).[33, 57] However, in methanol, the swelling ratio of P(MA-*co*-BPA) gel demonstrated a relatively large swelling ratio (327%) despite the relatively large $\Delta\delta_{p\text{-}s}$ compared to other solvents. As shown in **Figure 17a**, it was observed that P(MA-*co*-BPA) turned white when immersed in methanol, indicating that methanol was a non-solvent for P(MA-*co*-BPA). This abnormal swelling behavior seems to be due to the concentration-dependent diffusion of methanol into the cross-linked network of P(MA-*co*-BPA).[58, 59] As shown in **Figure 17b**, when Ti70 gel was immersed in pure commercial gasoline, methanol, xylene, toluene and benzene, the swelling ratios of Ti70 gel were 8%, 10%, 40%, 40%, and 41%, respectively, and it was confirmed that there are no difference in swelling ratio between dry gel and P(MA-*co*-BPA) gel.

As a result, when Ti70/P(MA-*co*-BPA) 1D PC was immersed in pure commercial gasoline, the thickness of the P(MA-*co*-BPA) layer hardly changed, but adulterants such as methanol, xylene, toluene and benzene added in adulterated gasoline, the thickness of the P(MA-*co*-BPA) layer increased significantly due to swelling, so this can be detected through the color change of 1D PC.

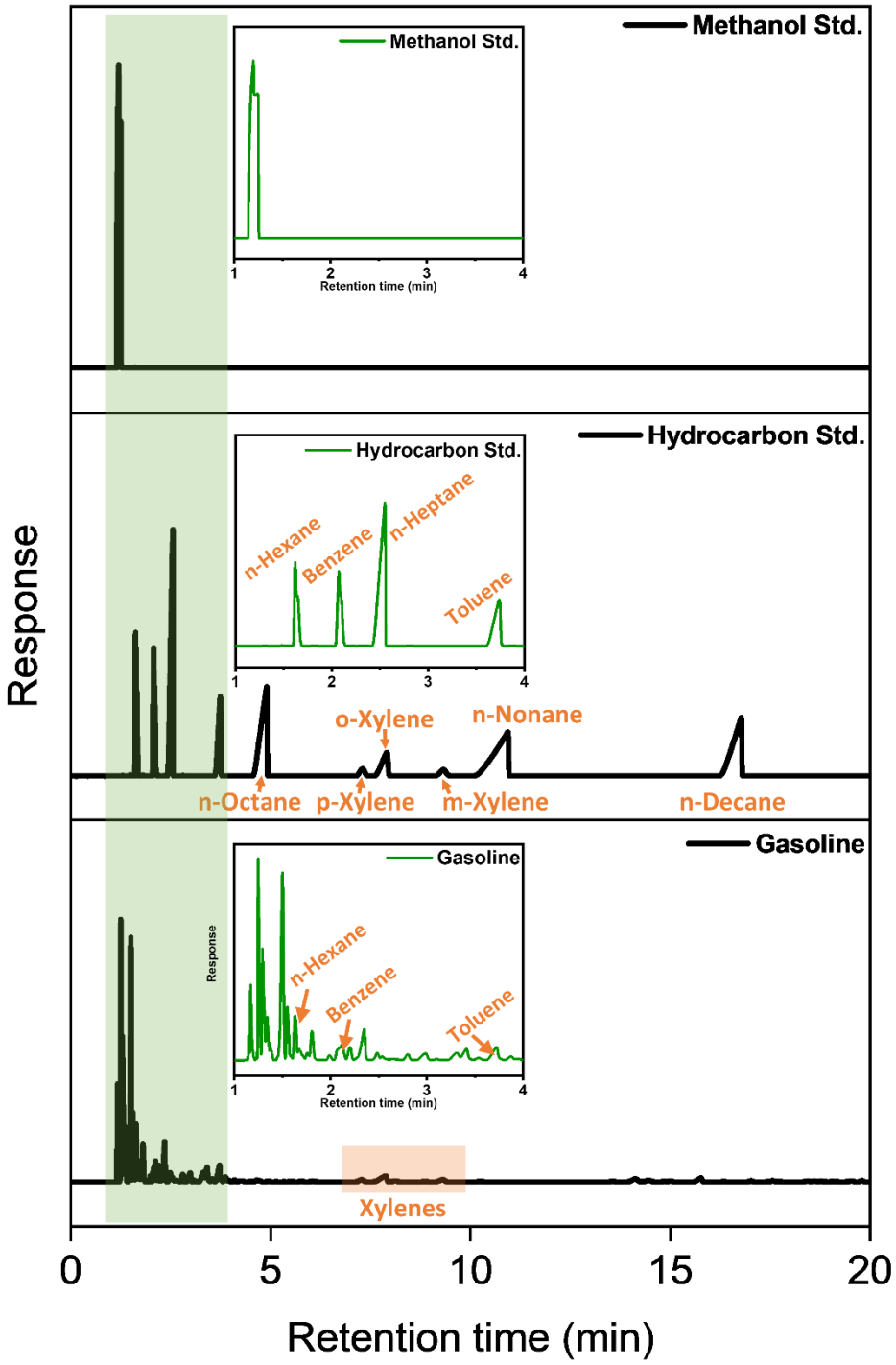

Figure 13. GC-FID results of gasoline, methanol, and hydrocarbon standards.

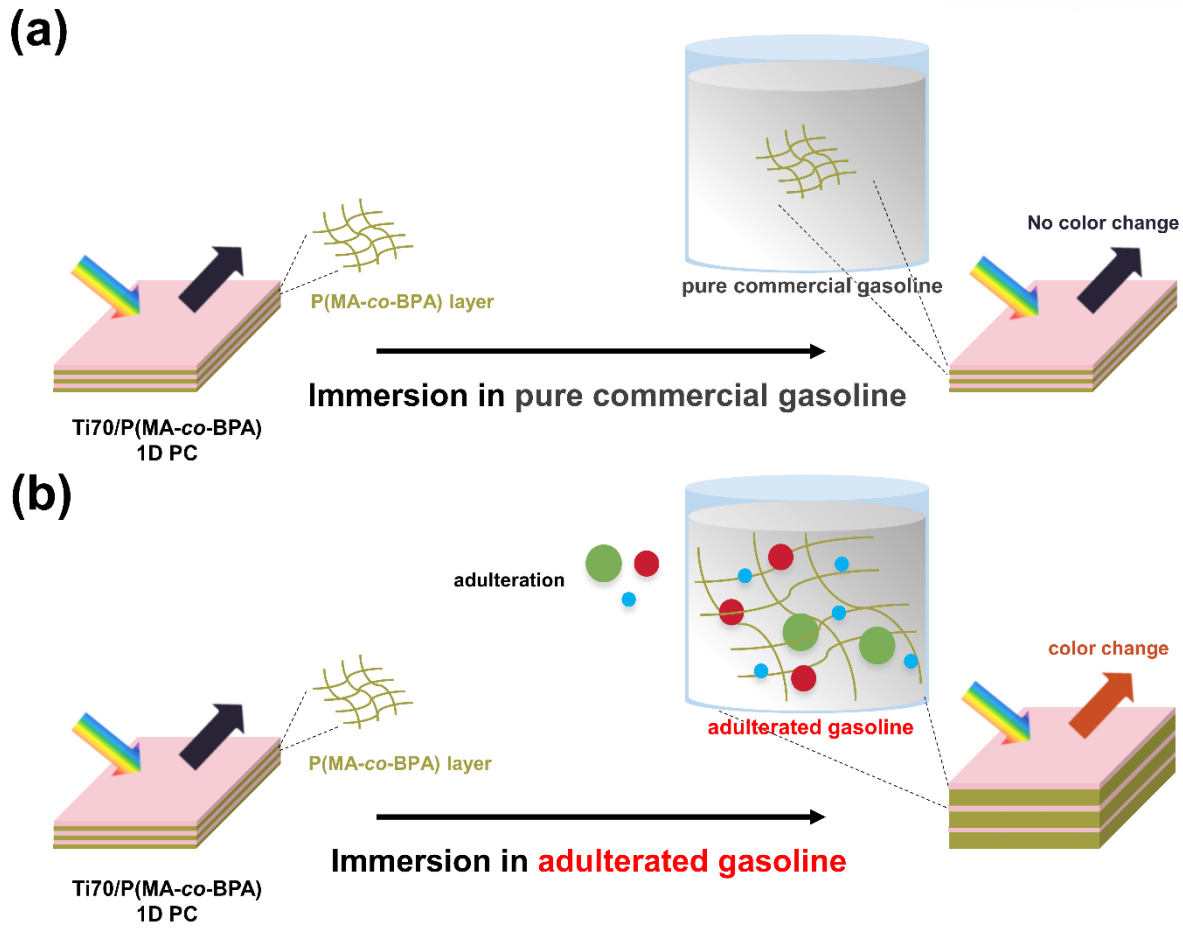

Figure 14. The appearance of a swelled film (a) when a Ti70/P(MA-*co*-BPA) 1D PC was immersed in pure commercial gasoline and (b) when it was immersed in adulterated gasoline.

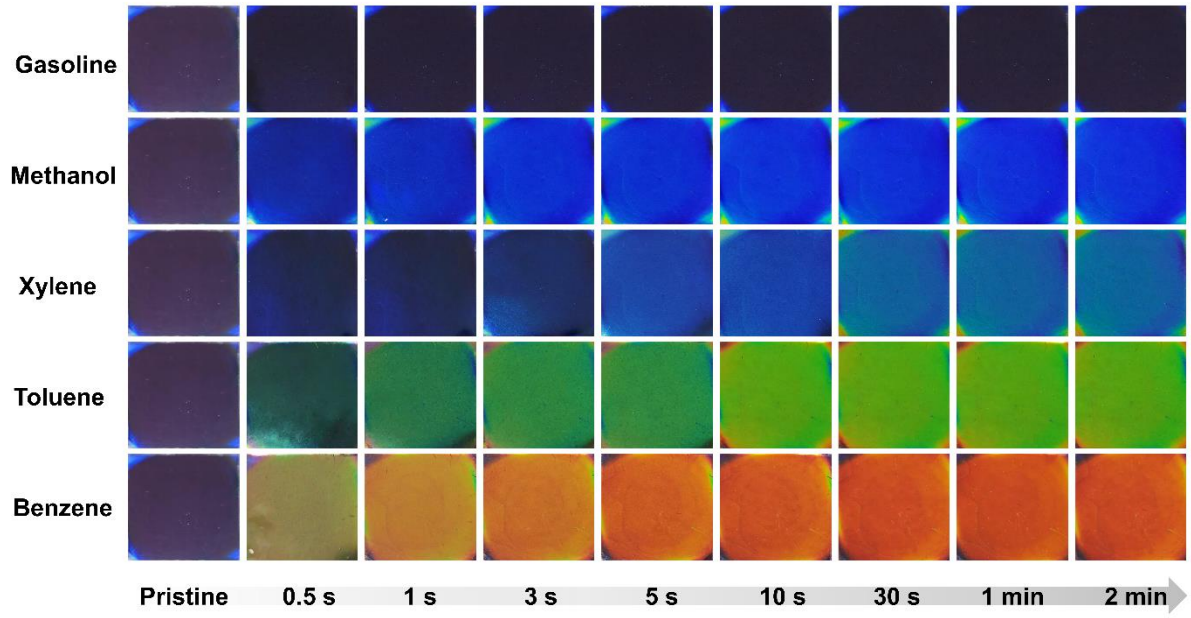

Figure 15. Image of color change with time when Ti70/P(MA-*co*-BPA) 1D PC was immersed in gasoline, methanol, xylene, toluene, and benzene.

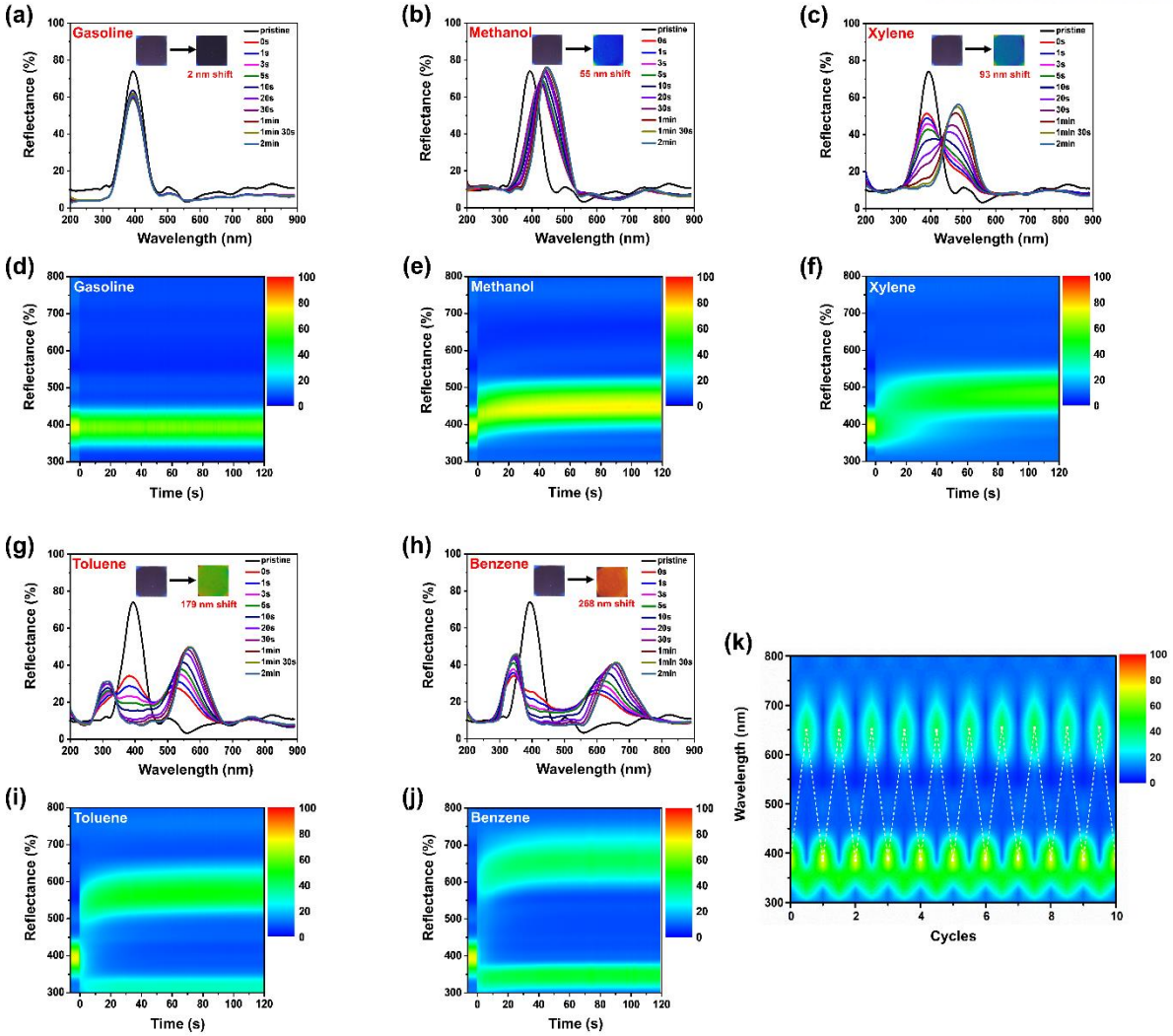

Figure 16. Changes in reflectance for 2 min of Ti70/P(MA-*co*-BPA) 1D PC when immersed in (a) gasoline, (b) methanol, (c) xylene, (g) toluene, (h) benzene and contour plots of (d) commercial gasoline, (e) methanol, (f) xylene, (i) toluene, (j) benzene, and (k) when immersed in benzene repeatedly 10 times.

Table 4. Molar volume (V_m), solubility parameters (δ_t) of P(MA-*co*-BPA) and solvents, and difference in solubility parameters between P(MA-*co*-BPA) and solvents for Hildebrand solubility parameters.

	Hildeband Solubility parameter		
	V_m (cm^3/mol)	δ_t ($Mpa^{1/2}$)	$\Delta\delta_{p\text{-}s}$[a] (between P(MA-*co*-BPA) and solvent)
P(MA-*co*-BPA)	-	19.1[b]	-
Gasoline	-	16.0[c]	3.1
Methanol[d]	40.5	29.6	10.5
Xylene[e]	122.9	18.0	1.1
Toluene[f]	106.9	18.2	0.9
Benzene[f]	89.4	18.4	0.7

[a] $\Delta\delta_{p\text{-}s}$ was difference in solubility parameter of P(MA-*co*-BPA) and solvent.
[b] δ_t of P(MA-*co*-BPA) was obtained from literature.[52]
[c] δ_t of gasoline was obtained from literature.[60]
[d] Data of methanol were obtained from literature.[56, 61]
[e] Data of xylene was a mean value of three isomers (ortho-, metha-, and para-isomer) obtained from literature.[54, 55]
[f] Data of toluene and benzene were obtained from literature.[55, 62, 63]

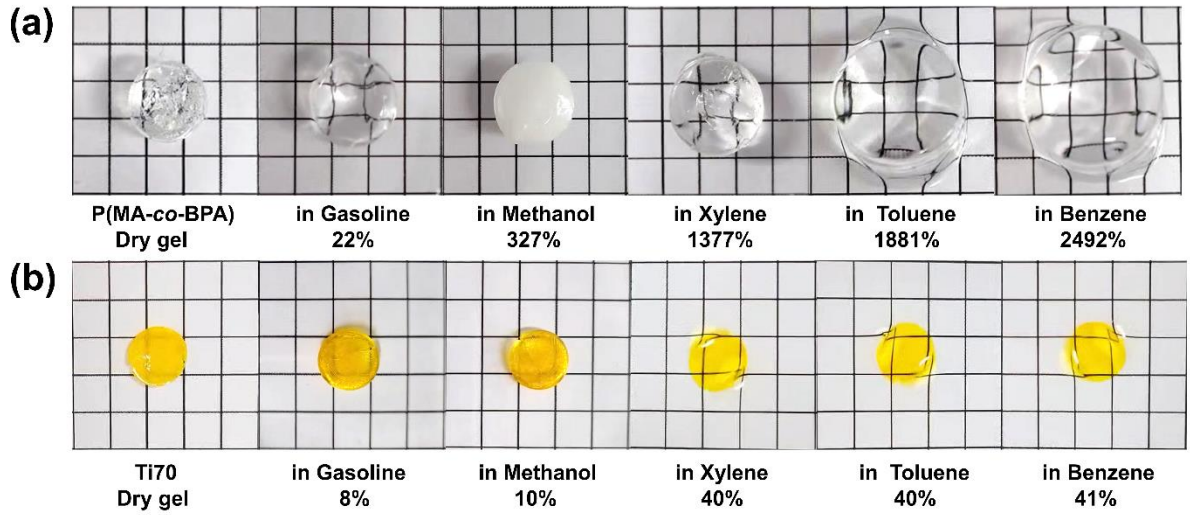

Figure 17. (a) P(MA-*co*-BPA) gel and (b) Ti70 gel swelled when immersed in pure commercial gasoline, methanol, xylene, toluene, and benzene, and the difference in weight content between dry gel and the swollen gel was calculated by **Equation (3)**.

3.5. Application of Ti70/P(MA-*co*-BPA) 1D PC

Using these properties, Ti70/P(MA-*co*-BPA) 1D PC was also tested on adulterated gasoline. The solvents commonly used as adulterants in adulterated gasoline are toluene and methanol.[7, 9, 10]

First, changes in reflectance and wavelength were observed when gasoline and toluene were mixed in different volume ratios (*v*:*v*) and immersed in Ti70/P(MA-*co*-BPA) 1D PC for 2 min (**Figure 18**). When a Ti70/P(MA-*co*-BPA) 1D PC was immersed in a gasoline and toluene mixture (GT mixture), the change in PSB peak wave length at 9:1, 8:2, 7:3, 6:4, 5:5, 4:6, 3:7, 2:8, and 1:9 (*v*:*v*) shifted to 7 nm, 9 nm, 19 nm, 43 nm, 63 nm, 98 nm, 107 nm, 129 nm, and 151 nm, respectively (**Figure 18a-i**). All PSB spectral shifts were saturated within 2 min. In Ti70/P(MA-*co*-BPA) 1D PC, as the volume ratio of toluene in the GT mixture increased, the expansion of the P(MA-*co*-BPA) layer increased and red shifted, and the reflectance was almost the same regardless of the volume ratio (57-61%). Therefore, this result confirmed that the toluene contained in the GT mixture can be sensitively detected with the naked-eye due to the swelling of Ti70/P(MA-*co*-BPA) 1D PC. Next, changes in reflectance and wavelength were observed when gasoline and methanol were mixed in different volume ratios (*v*:*v*) and immersed in Ti70/P(MA-*co*-BPA) 1D PC for 2 min (**Figure 19**).

When Ti70/P(MA-*co*-BPA) 1D PC was immersed in gasoline and methanol mixture (GM mixture), the changes in PSB peak wave lengths at 9:1, 8:2, 7:3, 6:4, 5:5, 4:6, 3:7, 2:8, and 1:9 (*v*:*v*) shifted to 59 nm, 60 nm, 61 nm, 64 nm, 69 nm, 69 nm, 69 nm, 67 nm, and 65 nm, respectively (**Figure 19a-i**). The reflectance of Ti70/P(MA-*co*-BPA) 1D PC increased from 62% to 76% when immersed in the GM mixture. All PSB spectral shifts were saturated within 1 min 30 s, and the PSB peak exhibited the same for Ti70/P(MA-*co*-BPA) 1D PC regardless of the volume ratio of methanol in the GM mixture. In addition, it was observed that the reflectance of Ti70/P(MA-*co*-BPA) 1D PC hardly decreased when immersed in GM mixture. This result is presumably because the abnormal non-solvent swelling of the P(MA-*co*-BPA) layers by methanol has little effect on the structural periodicity or defect generation of Ti70/P(MA-*co*-BPA) 1D PC. As a result, it was confirmed that methanol contained in the GM mixture can also be sensitively detected with the naked eye due to the non-solvent swelling of Ti70/P(MA-*co*-BPA) 1D PC.

On the other hand, more than one adulterant can be used for the actually used adulterated gasoline.[7, 9, 10] Therefore, the field usability of adulterated gasoline was explored by immersing Ti70/P(MA-*co*-BPA) 1D PC in gasoline, toluene, and methanol mixture (GTM mixture) (**Figure 20**). When gasoline, toluene, and methanol were mixed in different volume ratios (*v*:*v*:*v*) and Ti70/P(MA-*co*-BPA) 1D PC was immersed for 2 min, changes in reflectance and wavelength were observed (**Figure 20a-c**). When Ti70/P(MA-*co*-BPA) 1D PC was immersed in GTM mixture, the changes in PSB peak wave length at 8:1:1, 6:2:2, and 4:3:3 (*v*:*v*:*v*) shifted to 77 nm, 116 nm, and 160 nm, respectively. The spectral changes

in the GTM mixture of Ti70/P(MA-*co*-BPA) 1D PC can be interpreted by comparing the results of the GT mixture and the GM mixture. In GTM mix, methanol appeared to have a greater effect on the reflective color change of Ti70/P(MA-*co*-BPA) 1D PC at 8:1:1 (*v*:*v*:*v*). In the GTM mixture, methanol seemed to have a greater effect on the specular color change of Ti70/P(MA-*co*-BPA) 1D PC at 8:1:1 (*v*:*v*:*v*). This is because, as observed in the GM mixture, methanol induces about 65 nm red shifts in Ti70/P(MA-*co*-BPA) 1D PC regardless of the volume ratio. On the other hand, in the GTM mixture of 6:2:2, 4:3:3 (*v*:*v*:*v*) with an increased volume ratio of toluene, swelling by toluene induced additional spectral red shifts. In addition, as the volume ratio of toluene in the GTM mixture increased, a decrease in the reflectance of Ti70/P(MA-*co*-BPA) 1D PC was observed. It is previously confirmed that methanol does not break the periodicity of Ti70/P(MA-*co*-BPA) 1D PC. Therefore, this result can be interpreted as the swelling of the P(MA-*co*-BPA) layers, which increased as the volume ratio of toluene to the GTM mixture, broke the structural periodicity of Ti70/P(MA-*co*-BPA) 1D PC or created a defect. As a result, it was confirmed that adulterated gasoline containing toluene and methanol can be visually detected colorimetrically using Ti70/P(MA-*co*-BPA) 1D PC.

In addition, the shape of Ti70/P(MA-*co*-BPA) 1D PC can be easily modified by various shaping methods such as physical cutting and UV etching using a photo mask. As a simple example, a crown-shaped mask was attached to a Ti70/P(MA-*co*-BPA) 1D PC and used for visual detection of adulterated gasoline. As shown in **Figure 20d**, when a crown-shaped Ti70/P(MA-*co*-BPA) 1D PC was immersed in GTM mixtures of 8:1:1, 6:2:2, and 4:3:3 (*v*:*v*:*v*), it was observed that the reflection color changed to strong blue, blue, and yellow-green, respectively. As a result, it was confirmed that although Ti70/P(MA-*co*-BPA) 1D PC cannot selectively detect only certain substances among adulterants in adulterated gasoline, it can detect all adulterants sensitively.

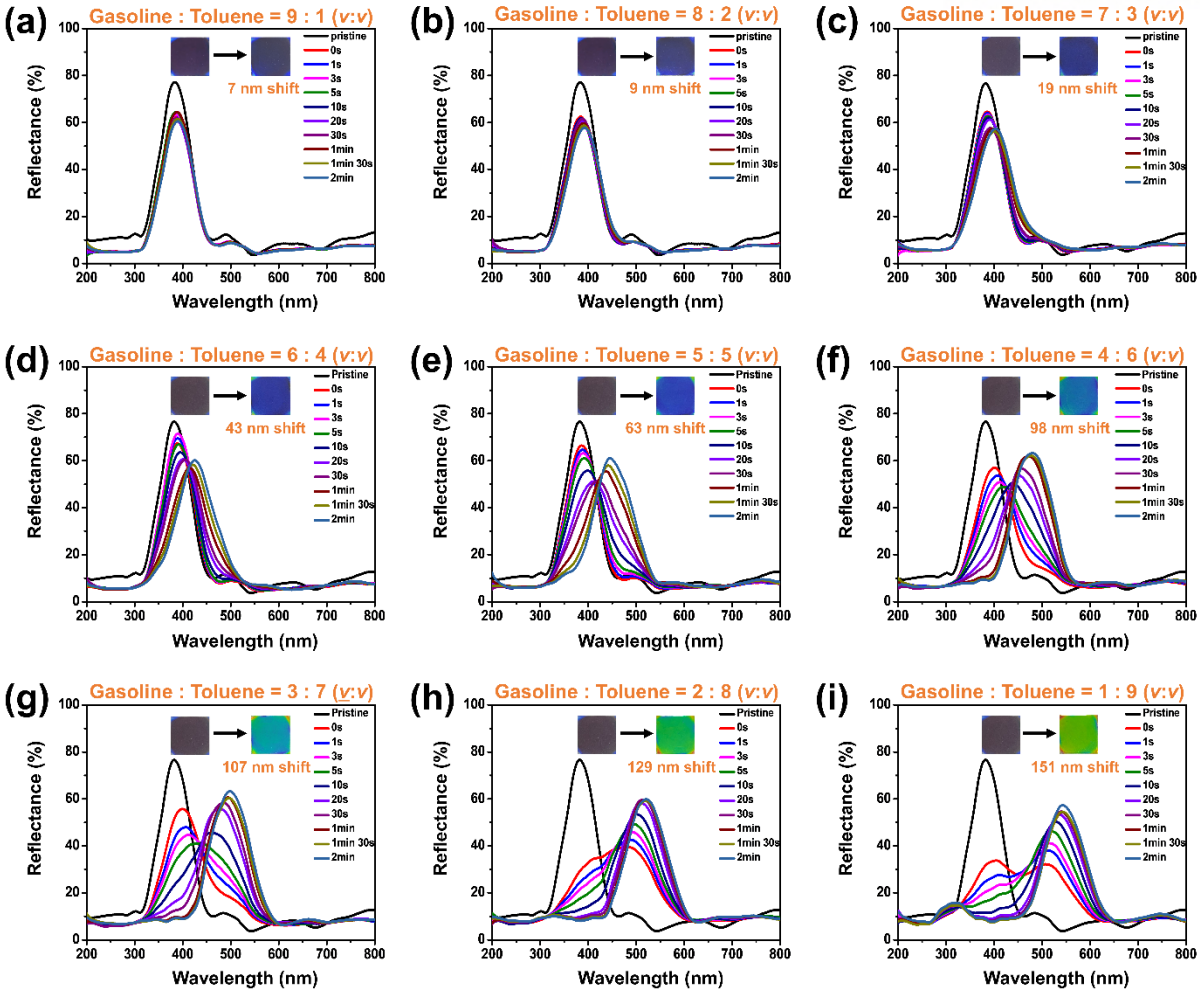

Figure 18. Reflectance and wavelength changes when Ti70/P(MA-*co*-BPA) 1D PC was immersed for 2 min by volume ratio of (a) 9:1, (b) 8:2, (c) 7:3, (d) 6:4, (e) 5:5, (f) 4:6, (g) 3:7, (h) 2:8, (i) 1:9 of gasoline : toluene.

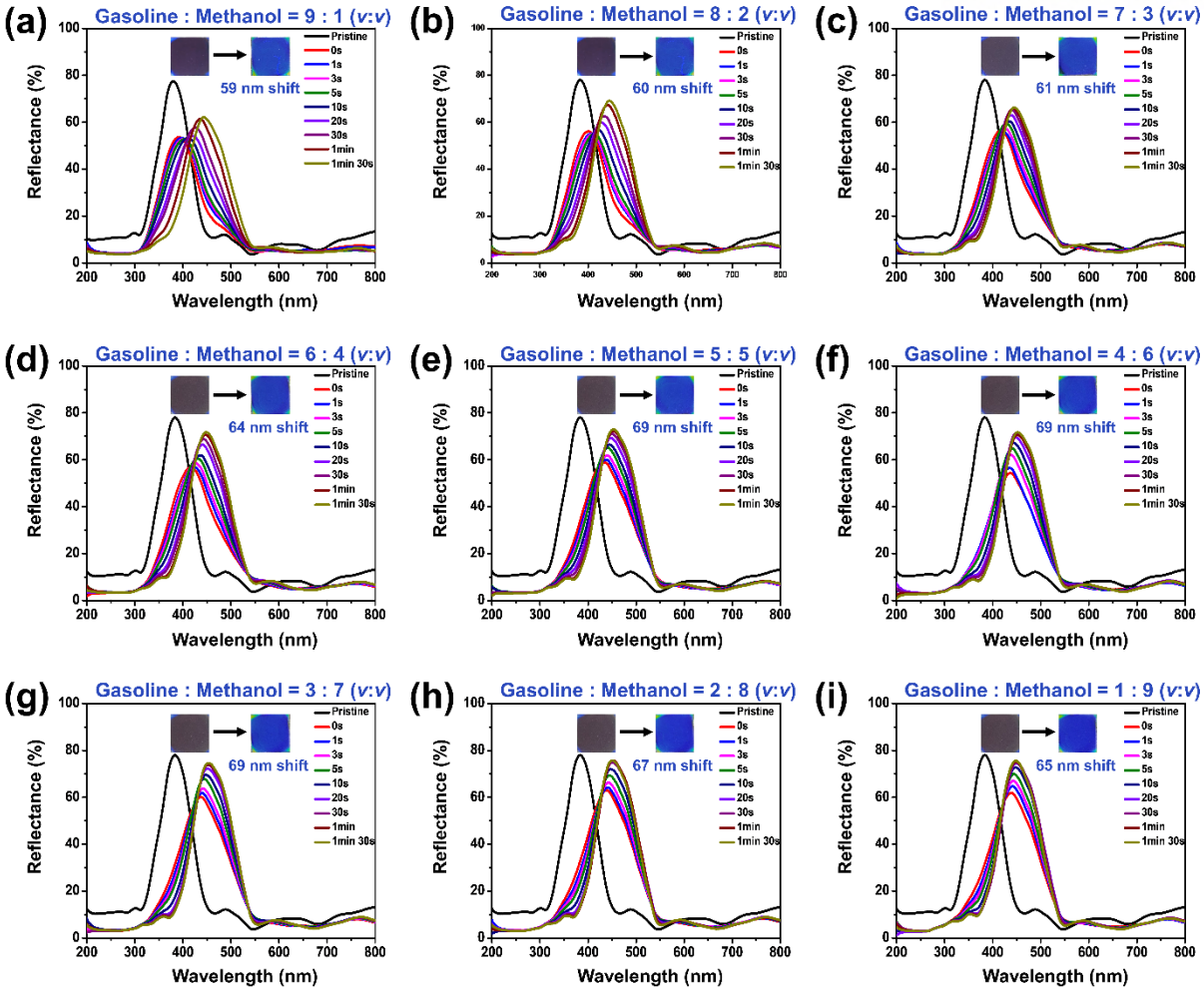

Figure 19. Reflectance and wavelength changes when Ti70/P(MA-*co*-BPA) 1D PC was immersed for 1 min 30 s by volume ratio of (a) 9:1, (b) 8:2, (c) 7:3, (d) 6:4, (e) 5:5, (f) 4:6, (g) 3:7, (h) 2:8, (i) 1:9 of gasoline : methanol.

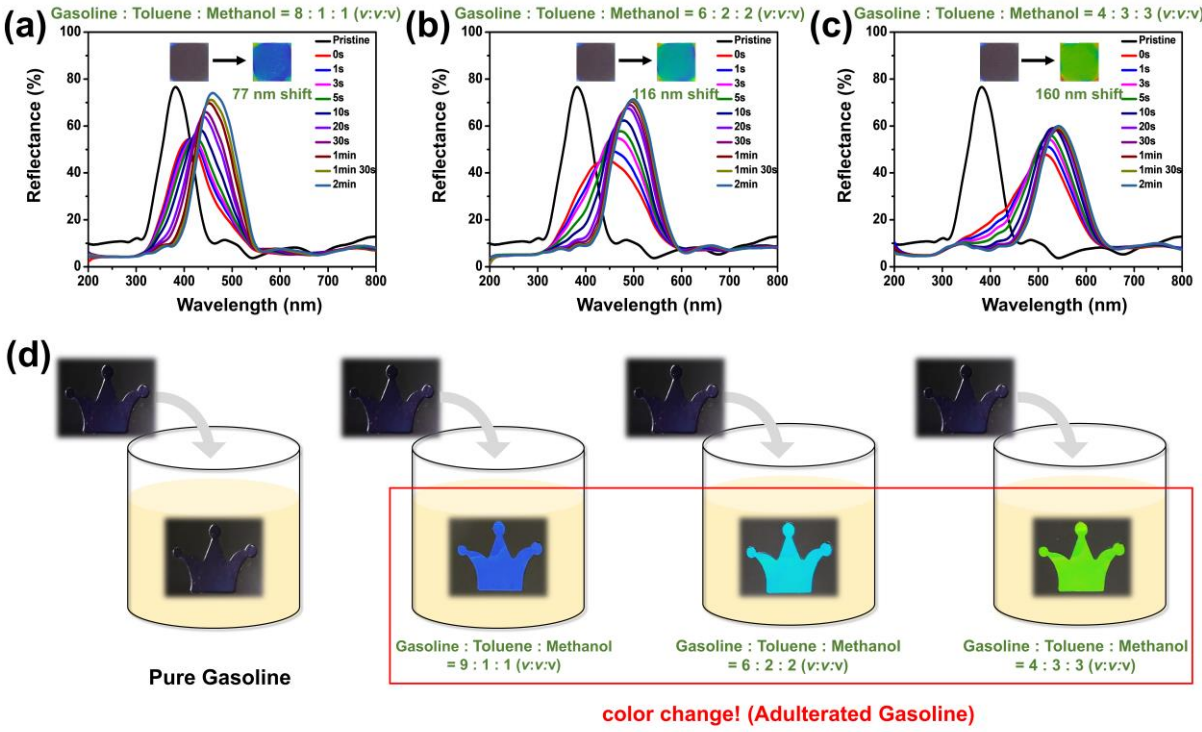

Figure 20. Reflectance and wavelength changes when Ti70/P(MA-*co*-BPA) 1D PC was immersed for 2 min by volume ratio of (a) 8:1:1, (b) 6:2:2, (c) 4:3:3 of gasoline : toluene : methanol and (d) images of distinguishing pure and adulterated gasoline when a crown shape film was put into unknown gasoline.

IV. Conclusion

Through this study, a highly reflective 1D PC sensor (Ti70/P(MA-*co*-BPA) 1D PC) was fabricated that can colorimetrically detect pure commercial gasoline and adulterated gasoline mixed with adulterants such as toluene and methanol. To this end, new polymeric-inorganic hybrids (Ti70) and P(MA-*co*-BPA) were synthesized, characterized, and used as HRIM and LRIM in the fabrication of a total of 11 layers of Ti70/P(MA-*co*-BPA) 1D PC, respectively. Ti70/P(MA-*co*-BPA) 1D PC exhibited a purple reflective color in pristine and no color change was observed when immersed in pure commercial gasoline. However, the Ti70/P(MA-*co*-BPA) 1D PC color changed rapidly to strong blue, blue, yellow-green, and orange within 10 s when it was immersed in methanol, xylene, toluene, and benzene, respectively, and also turned blue and yellow-green when it was immersed in adulterated gasoline mixed with toluene and methanol. This result was confirmed because the P(MA-*co*-BPA) layers exhibited changes in swelling behavior in various solvents. In addition, Ti70/P(MA-*co*-BPA) 1D PC showed excellent recyclability in repeated swelling/deswelling. Based on these results, it was confirmed that the developed Ti70/P(MA-*co*-BPA) 1D PC can successfully detect adulterated gasoline on-the-spot. Although the visual detection characteristics of the adulterated gasoline of Ti70/P(MA-*co*-BPA) 1D PC were evaluated using only certain model solvents, it is assumed that it can be sufficiently applied to the detection of a wider variety of adulterants considering the excellent solvent swelling characteristics of the P(MA-*co*-BPA) layer. In conclusion, the results of this study are expected to be the basis for the development of a simple and reliable 1D PC sensor that can detect various analytes.

References

(1) Steffen, B.; Patt, A. A historical turning point? Early evidence on how the Russia-Ukraine war changes public support for clean energy policies. Energy Research & Social Science 2022, 91, 102758.

(2) Zhou, X.-Y.; Lu, G.; Xu, Z.; Yan, X.; Khu, S.-T.; Yang, J.; Zhao, J. Influence of Russia-Ukraine War on the Global Energy and Food Security. Resources, Conservation and Recycling 2023, 188, 106657.

(3) Verma, G.; Prasad, R. K.; Agarwal, R. A.; Jain, S.; Agarwal, A. K. Experimental investigations of combustion, performance and emission characteristics of a hydrogen enriched natural gas fuelled prototype spark ignition engine. Fuel 2016, 178, 209-217. DOI: https://doi.org/10.1016/j.fuel.2016.03.022.

(4) Rosado, H. R. a. M. R. a. P. Energy. Our World in Data 2022.

(5) Qin, J.; Zhang, Z.; Li, Q.; Huang, J.; Peng, X.; Qing, L.; Liang, G.; Liang, L.; Huang, Y.; Yang, X. Concentrations and potential health risks of methyl tertiary-butyl ether (MTBE) in air and drinking water from Nanning, South China. Science of the Total Environment 2016, 541, 1348-1354.

(6) Correia, R. M.; Domingos, E.; Cáo, V. M.; Araujo, B. R.; Sena, S.; Pinheiro, L. U.; Fontes, A. M.; Aquino, L. F. M.; Ferreira, E. C.; Filgueiras, P. R. Portable near infrared spectroscopy applied to fuel quality control. Talanta 2018, 176, 26-33.

(7) Lee, J.; Balakrishnan, S.; Cho, J.; Jeon, S.-H.; Kim, J.-M. Detection of adulterated gasoline using colorimetric organic microfibers. Journal of Materials Chemistry 2011, 21 (8), 2648-2655.

(8) Vempatapu, B. P.; Kanaujia, P. K. Monitoring petroleum fuel adulteration: A review of analytical methods. TrAC Trends in Analytical Chemistry 2017, 92, 1-11. DOI: https://doi.org/10.1016/j.trac.2017.04.011.

(9) Lee, D.-M.; Lee, D.-H.; Hwang, I.-H. Gasoline quality assessment using fast gas chromatography and partial least-squares regression for the detection of adulterated gasoline. Energy & Fuels 2018, 32 (10), 10556-10562.

(10) Kock, F. V.; Rocha, T. C.; Araujo, G. M.; Simoes, F. R.; Colnago, L. A.; Barbosa, L. L. Time-domain NMR: A novel analytical method to quantify adulteration of ethanol fuel with methanol. Fuel 2019, 258, 116158.

(11) Duan, C.; Li, J.; Zhang, Y.; Ding, K.; Geng, X.; Guan, Y. Portable instruments for on-site analysis of environmental samples. TrAC Trends in Analytical Chemistry 2022, 116653.

(12) Fan, J.; Qiu, L.; Qiao, Y.; Xue, M.; Dong, X.; Meng, Z. Recent Advances in Sensing Applications of Molecularly Imprinted Photonic Crystals. Frontiers in Chemistry 2021, 237.

(13) Maeng, B.; Chang, H.-k.; Park, J. Photonic crystal-based smart contact lens for continuous intraocular pressure monitoring. Lab on a Chip 2020, 20 (10), 1740-1750.

(14) Wang, F.; Meng, Z.; Xue, F.; Xue, M.; Lu, W.; Chen, W.; Wang, Q.; Wang, Y. Responsive photonic crystal for the sensing of environmental pollutants. Trends in Environmental Analytical Chemistry 2014, 3, 1-6.

(15) da Nóbrega Gaiao, E.; dos Santos, S. R. B.; dos Santos, V. B.; do Nascimento, E. C. L.; Lima, R. S.; de Araújo, M. C. U. An inexpensive, portable and microcontrolled near infrared LED-photometer for screening analysis of gasoline. Talanta 2008, 75 (3), 792-796.

(16) Gotor, R.; Bell, J.; Rurack, K. Tailored fluorescent solvatochromic test strips for quantitative on-

site detection of gasoline fuel adulteration. Journal of Materials Chemistry C 2019, 7 (8), 2250-2256.

(17) Bordbar, M. M.; Tashkhourian, J.; Hemmateenejad, B. Based Optical Nose Made with Bimetallic Nanoparticles for Monitoring Ignitable Liquids in Gasoline. ACS Applied Materials & Interfaces 2022, 14 (6), 8333-8342.

(18) Kim, J. M.; Jung, Y. J.; Park, B. C.; Lim, B.; Kong, H.; Park, J. M.; Lee, H.-i.; Jung, S.-H. Photonic multilayers for ultrasensitive millisecond colorimetric discrimination between benzene, toluene, and xylene. Sensors and Actuators B: Chemical 2022, 351, 130974.

(19) Kou, D.; Ma, W.; Zhang, S.; Tang, B. Copolymer-based photonic crystal sensor for discriminative detection of liquid benzene, toluene, ethylbenzene, and xylene. ACS Applied Polymer Materials 2019, 2 (1), 2-11.

(20) Kou, D.; Zhang, Y.; Zhang, S.; Wu, S.; Ma, W. High-sensitive and stable photonic crystal sensors for visual detection and discrimination of volatile aromatic hydrocarbon vapors. Chemical Engineering Journal 2019, 375, 121987.

(21) Däntl, M.; Jiménez-Solano, A.; Lotsch, B. V. Stimuli-Responsive One-Dimensional Photonic Crystals: Design, Fabrication and Sensing. Materials Advances 2022.

(22) John, S.; Joannopoulos, D.; Winn, J. N.; Meade, R. D. Photonic crystals: molding the flow of light. InPrinceton University of Press: Princeton, NJ, USA 2008.

(23) Shen, H.; Wang, Z.; Wu, Y.; Yang, B. One-dimensional photonic crystals: fabrication, responsiveness and emerging applications in 3D construction. RSC advances 2016, 6 (6), 4505-4520.

(24) Wu, Z.; Lee, D.; Rubner, M. F.; Cohen, R. E. Structural color in porous, superhydrophilic, and self-cleaning SiO2/TiO2 Bragg stacks. Small 2007, 3 (8), 1445-1451.

(25) Fathi, F.; Rashidi, M.-R.; Pakchin, P. S.; Ahmadi-Kandjani, S.; Nikniazi, A. Photonic crystal based biosensors: Emerging inverse opals for biomarker detection. Talanta 2021, 221, 121615.

(26) Yoshioka, S.; Kinoshita, S. Wavelength–selective and anisotropic light–diffusing scale on the wing of the Morpho butterfly. Proceedings of the Royal Society of London. Series B: Biological Sciences 2004, 271 (1539), 581-587.

(27) Vukusic, P.; Sambles, J. R. Photonic structures in biology. Nature 2003, 424 (6950), 852-855.

(28) Yoshioka, S.; Kinoshita, S. Effect of macroscopic structure in iridescent color of the peacock feathers. FORMA-TOKYO- 2002, 17 (2), 169-181.

(29) Zhao, Q.; Wang, Y.; Cui, H.; Du, X. Bio-inspired sensing and actuating materials. Journal of Materials Chemistry C 2019, 7 (22), 6493-6511.

(30) Das, S.; Shanmugam, N.; Kumar, A.; Jose, S. Potential of biomimicry in the field of textile technology. Bioinspired, Biomimetic and Nanobiomaterials 2017, 6 (4), 224-235.

(31) Lova, P.; Manfredi, G.; Comoretto, D. Advances in functional solution processed planar 1D photonic crystals. Advanced Optical Materials 2018, 6 (24), 1800730.

(32) Kou, D.; Zhang, S.; Lutkenhaus, J. L.; Wang, L.; Tang, B.; Ma, W. Porous organic/inorganic hybrid one-dimensional photonic crystals for rapid visual detection of organic solvents. Journal of Materials Chemistry C 2018, 6 (11), 2704-2711.

(33) Wang, L.; Zhang, S.; Lutkenhaus, J. L.; Chu, L.; Tang, B.; Li, S.; Ma, W. All nanoparticle-based P (MMA–AA)/TiO 2 one-dimensional photonic crystal films with tunable structural colors. Journal of

Materials Chemistry C 2017, 5 (32), 8266-8272.

(34) Dou, Y.; Han, J.; Wang, T.; Wei, M.; Evans, D. G.; Duan, X. Fabrication of MMO–TiO 2 one-dimensional photonic crystal and its application as a colorimetric sensor. Journal of Materials Chemistry 2012, 22 (28), 14001-14007.

(35) Mir, S. H.; Nagahara, L. A.; Thundat, T.; Mokarian-Tabari, P.; Furukawa, H.; Khosla, A. Organic-inorganic hybrid functional materials: An integrated platform for applied technologies. Journal of The Electrochemical Society 2018, 165 (8), B3137.

(36) Richert, L.; Boulmedais, F.; Lavalle, P.; Mutterer, J.; Ferreux, E.; Decher, G.; Schaaf, P.; Voegel, J.-C.; Picart, C. Improvement of stability and cell adhesion properties of polyelectrolyte multilayer films by chemical cross-linking. Biomacromolecules 2004, 5 (2), 284-294.

(37) Colodrero, S.; Ocaña, M.; González-Elipe, A. R.; Míguez, H. Response of nanoparticle-based one-dimensional photonic crystals to ambient vapor pressure. Langmuir 2008, 24 (16), 9135-9139.

(38) Liu, F.; Jiang, S.; Ionov, L.; Agarwal, S. Thermophilic films and fibers from photo cross-linkable UCST-type polymers. Polymer Chemistry 2015, 6 (14), 2769-2776.

(39) Vatankhah-Varnoosfaderani, M.; Hashmi, S.; GhavamiNejad, A.; Stadler, F. J. Rapid self-healing and triple stimuli responsiveness of a supramolecular polymer gel based on boron–catechol interactions in a novel water-soluble mussel-inspired copolymer. Polymer Chemistry 2014, 5 (2), 512-523.

(40) Lee, H.; Lee, B. P.; Messersmith, P. B. A reversible wet/dry adhesive inspired by mussels and geckos. Nature 2007, 448 (7151), 338-341.

(41) Patil, N.; Falentin-Daudré, C.; Jérôme, C.; Detrembleur, C. Mussel-inspired protein-repelling ambivalent block copolymers: controlled synthesis and characterization. Polymer Chemistry 2015, 6 (15), 2919-2933.

(42) Nishida, J.; Kobayashi, M.; Takahara, A. Gelation and adhesion behavior of mussel adhesive protein mimetic polymer. Journal of Polymer Science Part A: Polymer Chemistry 2013, 51 (5), 1058-1065.

(43) Liou, G. S.; Lin, P. H.; Yen, H. J.; Yu, Y. Y.; Chen, W. C. Flexible nanocrystalline-titania/polyimide hybrids with high refractive index and excellent thermal dimensional stability. Journal of Polymer Science Part A: Polymer Chemistry 2010, 48 (6), 1433-1440.

(44) Hara, S.; Tomono, M.; Fukumoto, K.; Kubodera, M.; Kato, N.; Kaneko, T.; Toyama, T.; Shimizu, S.; Ikake, H. Melt-Moldable Copolymethacrylate/Titania Thermoreversible Polymer Networks with Shape Memory. ACS Applied Polymer Materials 2020, 2 (12), 5654-5663.

(45) Hara, S.; Aisu, J.; Nishizaki, Y.; Kato, H.; Sanae, G.; Kurebayashi, S.; Shimizu, S.; Ikake, H. Bulk structure of poly (ethylene glycol)/Titania hybrid system and the evaluation of their influence on apatite growth using simulated body fluid (SBF). Polymer Testing 2021, 94, 106984.

(46) Su, H.-W.; Chen, W.-C. High refractive index polyimide–nanocrystalline-titania hybrid optical materials. Journal of Materials Chemistry 2008, 18 (10), 1139-1145.

(47) Lim, K. S.; Klotz, B. J.; Lindberg, G. C.; Melchels, F. P.; Hooper, G. J.; Malda, J.; Gawlitta, D.; Woodfield, T. B. Visible light cross-linking of gelatin hydrogels offers an enhanced cell microenvironment with improved light penetration depth. Macromolecular bioscience 2019, 19 (6), 1900098.

(48) Einzinger, M.; Wu, T.; Kompalla, J. F.; Smith, H. L.; Perkinson, C. F.; Nienhaus, L.; Wieghold, S.;

Congreve, D. N.; Kahn, A.; Bawendi, M. G. Sensitization of silicon by singlet exciton fission in tetracene. Nature 2019, 571 (7763), 90-94.

(49) Backes, S.; Krause, P.; Tabaka, W.; Witt, M. U.; Mukherji, D.; Kremer, K.; von Klitzing, R. Poly (N-isopropylacrylamide) microgels under alcoholic intoxication: When a lcst polymer shows swelling with increasing temperature. ACS Macro Letters 2017, 6 (10), 1042-1046.

(50) Nash, M. E.; Healy, D.; Carroll, W. M.; Elvira, C.; Rochev, Y. A. Cell and cell sheet recovery from pNIPAm coatings; motivation and history to present day approaches. Journal of Materials Chemistry 2012, 22 (37), 19376-19389.

(51) Su, R.; Liu, G.; Sun, H.; Yong, Z. A new method to measure the three-dimensional solubility parameters of acrylate rubber and predict its oil resistance. Polymer Bulletin 2022, 79 (2), 971-984.

(52) Lindvig, T.; Michelsen, M. L.; Kontogeorgis, G. M. A Flory–Huggins model based on the Hansen solubility parameters. Fluid Phase Equilibria 2002, 203 (1-2), 247-260.

(53) Praveen, P.; Viruthagiri, G.; Mugundan, S.; Shanmugam, N. Structural, optical and morphological analyses of pristine titanium di-oxide nanoparticles – Synthesized via sol–gel route. Spectrochimica Acta Part A: Molecular and Biomolecular Spectroscopy 2014, 117, 622-629. DOI: https://doi.org/10.1016/j.saa.2013.09.037.

(54) Zhu, Q.-N.; Wang, Q.; Hu, Y.-B.; Abliz, X. Practical determination of the solubility parameters of 1-alkyl-3-methylimidazolium bromide ([CnC1im] Br, n= 5, 6, 7, 8) ionic liquids by inverse gas chromatography and the Hansen solubility parameter. Molecules 2019, 24 (7), 1346.

(55) Jasem A. Al-Kandary, A. S. A.-J., and Abdul-Haq M. Abdul-Latif. Viscosities, Densities, and Speeds of Sound of Binary Mixtures of Benzene, Toluene, o-Xylene, m-Xylene, p-Xylene, and Mesitylene with Anisole at (288.15, 293.15, 298.15, and 303.15) K. Journal of Chemical & Engineering Data 2006, 51 (6), 2074-2082.

(56) Nguyen, T. V. N.; Paugam, L.; Rabiller, P.; Rabiller-Baudry, M. Study of transfer of alcohol (methanol, ethanol, isopropanol) during nanofiltration in water/alcohol mixtures. Journal of Membrane Science 2020, 601, 117907.

(57) Lee, J. N.; Park, C.; Whitesides, G. M. Solvent compatibility of poly (dimethylsiloxane)-based microfluidic devices. Analytical chemistry 2003, 75 (23), 6544-6554.

(58) Guo, H.; Nakajima, T.; Hourdet, D.; Marcellan, A.; Creton, C.; Hong, W.; Kurokawa, T.; Gong, J. P. Hydrophobic Hydrogels with Fruit-Like Structure and Functions. Advanced Materials 2019, 31 (25), 1900702.

(59) Shundo, A.; Hori, K.; Penaloza, D. P.; Yoshihiro, K.; Annaka, M.; Tanaka, K. Nonsolvents-induced swelling of poly (methyl methacrylate) nanoparticles. Physical Chemistry Chemical Physics 2013, 15 (39), 16574-16578.

(60) Kass, M. D.; Theiss, T.; Pawel, S.; Baustian, J.; Wolf, L.; Koch, W.; Janke, C. Compatibility assessment of elastomer materials to test fuels representing gasoline blends containing ethanol and isobutanol. SAE International Journal of Fuels and Lubricants 2014, 7 (2), 445-456.

(61) Hevia, F.; Alonso, V.; Cobos, A.; González, J. A.; Sanz, L. F.; de la Fuente, I. G. Density, speed of sound, refractive index and relative permittivity of methanol, propan-1-ol or pentan-1-ol+ benzylamine liquid mixtures. Application of the Kirkwood-Fröhlich model. The Journal of Chemical Thermodynamics 2022, 168, 106737.

(62) Hansen, C. M. The universality of the solubility parameter. Industrial & engineering chemistry

product research and development 1969, 8 (1), 2-11.

(63) Ho, D. L.; Glinka, C. J. Effects of solvent solubility parameters on organoclay dispersions. Chemistry of Materials 2003, 15 (6), 1309-1312.

Acknowledgement

This thesis is based on the previously published article ‘Hwang, T. G.; Jeong, M.; Park, J.; Jung, Y. J.; Hwang, D.-H.; Park, J. M., On-site colorimetric detection of adulterated gasoline using highly reflective 1D photonic crystal sensors based on photo-crosslinked polymer–titania hybrids. *Sensors and Actuators B: Chemical* 2022, 371, 132488.’ with permission from the Elsevier B.V.